Journal of Sound and Vibration 329 (2010) 4227–4250

Contents lists available at ScienceDirect

Journal of Sound and Vibration

journal homepage: www.elsevier.com/locate/jsvi

Sound radiation from perforated plates

A. Putra [1], D.J. Thompson *

Institute of Sound and Vibration Research, University of Southampton, Highfield, Southampton SO17 1BJ, UK

ARTICLE INFO

Article history:
Received 20 August 2009
Received in revised form
7 April 2010
Accepted 20 April 2010
Handling Editor: Y. Auregan
Available online 13 May 2010

ABSTRACT

A practical engineering noise control measure that can often be used for plate-like structures is to construct them from perforates. This can dramatically reduce the sound radiation from such structures. Here, a prediction model is developed to quantify this effect. It is an extension of Laulagnet's model for the radiation from an unbaffled plate, which expresses the surface pressure difference as well as the plate velocity as a sum over plate modes. The perforation is included in terms of a continuously distributed surface impedance, which for moderately sized holes is predominantly inertial. Results show that the radiation efficiency reduces, not only as the perforation ratio increases but also as the hole size reduces for a given perforation ratio. Experimental validation is given which shows a good agreement with the predictions. An approximate formula is also proposed for the effect of perforation which corresponds well with the analytical calculations up to half the critical frequency and could be used for an engineering application to predict the noise reduction due to perforation. A model for the case of a perforated plate embedded in an equally perforated baffle is also discussed for comparison.

1. Introduction

The vibration of engineering structures, particularly those consisting of thin plate-like members, can be a significant source of noise in many situations. Noise control techniques are often focussed on reducing the amplitudes of vibration and include damping treatments, vibration isolation and structural modification. However, it is sometimes also possible to reduce the sound radiation of plate-like structures directly by constructing them from perforates. This technique is known to be capable of achieving considerable noise reductions and has found many practical applications, including safety guard enclosures over flywheels or belt drives and product collection hoppers [1]. Despite this, there appears to be a lack of suitable models to determine the sound radiation from a vibrating perforated plate and to give quantitative guidance concerning the design and effectiveness of perforation as a noise control measure.

Fahy and Thompson [2] developed a model for the sound radiation by plane bending waves propagating in an unbounded, uniformly perforated plate. In this model the perforations are replaced by an equivalent continuous impedance, based on the assumption that the hole size and separation are much smaller than the acoustic wavelength. The acoustic impedance of each hole was represented by the analytical solution for wave propagation in a small circular tube, similar to that proposed by Maa [3], and was dominated by the inertia of the air in the holes.

The model was then applied to the case of a simply supported rectangular plate, in the same way as for a solid plate set in an infinite rigid baffle [4], by expanding the plate vibration in the wavenumber domain. Although this allowed the radiation efficiency of a finite plate to be determined, it was based on the assumption that the baffle had the same

* Corresponding author. Tel.: +44 23 8059 2294; fax: +44 23 8059 3190.
E-mail addresses: azma.putra@utem.edu.my (A. Putra), djt@isvr.soton.ac.uk (D.J. Thompson).
[1] Currently at Universiti Teknikal Malaysia Melaka (UTeM).

0022-460X/$ - see front matter © 2010 Elsevier Ltd. All rights reserved.
doi:10.1016/j.jsv.2010.04.020

impedance as the plate, which implied that the baffle was perforated in the same way as the plate. Thus the effect of plate perforation could not be seen unambiguously.

An extension of this model was also considered in which the plate and the baffle had different impedances [2]. The relation between the pressures and normal velocities was derived in the wavenumber domain as a matrix problem and solved by matrix inversion. This was applied to the one-dimensional case of the radiation from a perforated strip piston and good results were found for the case where it is set in a rigid baffle. However, as the impedance of the baffle tends towards that of the free medium, the matrix becomes near-singular giving erratic predictions. Moreover, expanding this approach to a two-dimensional case, such as a rectangular plate, is found to lead to excessive computational effort [5].

The problem of the sound radiation from an unbaffled plate is, in general, more difficult to solve than for a plate set in an infinite baffle, as the velocity is known only over the surface of the plate, whereas in the remainder of the plane the pressure is known (zero) and the velocity is unknown. Although various analytical methods exist for determining the sound radiation from an unbaffled flat plate [6–10], these are less well known and take much more computational effort than for the baffled plate. Of the various approaches in the literature, that developed by Laulagnet [10] is particularly relevant as it can be readily extended to the case of a perforated plate, as will be shown. Laulagnet's approach [10] involves solving the Kirchhoff–Helmholtz integral equation by expressing the plate displacement and also the pressure jump across the plate as a sum of normal modes of the plate.

There are few other models for the radiation from perforated plates. Janssens and van Vliet [11] produced a purely empirical model for the effect of perforation on the radiation efficiency of flat plates. This was intended for application to components of steel railway bridges.

According to the author's knowledge, the first analytical model of sound radiation from a vibrating perforated panel was published by Takahashi and Tanaka [12]. They presented the acoustic coupling of a perforated plate using Maa's impedance model for the holes [3] and used this to study several problems, including the sound radiation from an infinite perforated plate subjected to a point force. Their results suggested that the perforation affects the radiated power only below the panel critical frequency, where the sound power was found to decrease as the perforation ratio was increased.

This basic model was then adopted in [13,14] which considered the radiation from a force-excited plate in the presence of a perforated face plate, rigidly attached to the plate via a honeycomb spacer. A large reduction in sound radiation was obtained due to perforation of the facing plate in the narrow frequency band around the resonance of the Helmholtz resonator formed by the air cavity inside the honeycomb structure and the holes of the perforate.

There has been considerable interest recently in the performance of micro-perforated plates. These typically have holes with diameters in the range 0.05–1.0 mm and perforation ratios of 0.5–1.5 percent. Models for micro-perforates [15–18] are mostly aimed at predicting their acoustic absorption and use the impedance of Maa [3] to represent the holes. Due to the small size of the holes viscous effects are important. In [17], sound absorption from a finite micro-perforated plate is investigated where the effect of plate motion is included based on the approach from [12].

The effects of plate boundaries are expected to be important. Therefore, whereas Takahashi and Tanaka [12] consider a vibrating perforated plate of infinite extent, in the present paper models are developed for the sound radiation from finite perforated plates. The model from Fahy and Thompson [2] of a finite perforated plate set in an equally perforated infinite baffle is first presented. Then, the model of Laulagnet [10] for the radiation from an unbaffled plate is extended to include a surface impedance representing perforations. The results from these two models are compared. Experimental results are also presented for a number of perforated plates, showing good agreement with the predictions. An approximate formula is also derived from which the effect of perforation can be estimated for engineering application.

The paper focuses on perforated plates with hole diameters of the order of several millimetres, typically used in engineering applications, rather than on micro-perforates. Consequently inertial effects will dominate over viscous effects within the holes and the hole impedance can be represented simply by the inertial term, as used by Fahy and Thompson [2]. Therefore the model as presented here is not directly applicable to the case of a micro-perforated plate where the hole diameter is typically smaller than about 1 mm, although it could be readily extended to cover this case by including the additional viscous terms in the impedance.

2. Theory

2.1. Hole acoustic impedance

Models for sound radiation from a perforated plate can be developed by introducing the impedance of the holes to account for the change in pressure difference across the plate due to perforation. Consider first a single hole in a plate for a given frequency ω. The flow velocity through the hole v_h is related to the pressure difference across the hole Δp by the impedance of the hole, Z_h

$$v_h = \frac{\Delta p}{Z_h} \tag{1}$$

The impedance $Z_h = Z_{h,R} + Z_{h,I}$ of a circular hole of diameter d_0 is given by Maa [3]

$$Z_{h,R} = \frac{32 v_a t}{d_0^2}\left[\left(1+\frac{X_0^2}{32}\right)^{1/2} + \left(\frac{\sqrt{2}X_0}{8}\right)\frac{d_0}{t}\right] \tag{2}$$

$$Z_{h,I} = \mathrm{j}\rho\omega t\left[1+\left(9+\frac{X_0^2}{2}\right)^{-1/2} + \left(\frac{8}{3\pi}\right)\frac{d_0}{t}\right] \tag{3}$$

where $X_0 = (d_0/2)(\omega\rho/v_a)^{1/2}$ in which ρ is the air density and v_a is the viscosity (which for air is 1.8×10^{-5} N s/m^2), t is the plate thickness and a dependence on time T of $e^{j\omega T}$ is assumed. The resistive or real part of the impedance $Z_{h,R}$ corresponds to viscous effects of air–solid interaction, while the imaginary part $Z_{h,I}$, termed the acoustic reactance, is inertial in nature.

In fact, although the pressure difference due to inertial forces is indeed proportional to the fluid motion v_h, as indicated in Eq. (1), the viscous forces are proportional to the *relative* motion of the fluid with respect to the plate [12]. Strictly, therefore, it is not correct to use the above impedance for the case of a plate that is vibrating. Nevertheless, except for large perforation ratios the motion of the fluid will usually be much greater than that of the plate and this difference can be neglected.

Fig. 1 plots the real and imaginary parts of the acoustic impedance of 1 and 6 mm thick plates as a function of hole diameter for three example frequencies. This shows that, as the hole diameter becomes smaller, the contribution of the resistive component to the acoustic impedance becomes greater than that of the reactive component. Conversely, as the hole diameter increases, the resistive contribution decreases rapidly. Hence, it can be seen that, for hole diameters greater than about 1 mm, the reactive component dominates the acoustic impedance at frequencies of 100 Hz and greater. Therefore for the purpose of the present study, where d_0 is much greater than 1 mm, it can be assumed that the fluid reaction in the holes is purely inertial (behaves like a mass). Hence the resistive component $Z_{h,R}$ will be neglected, leaving only the reactive component $Z_{h,I}$ which can be simplified to

$$Z_h = Z_{h,I} = \mathrm{j}\rho\omega\left[t+\left(\frac{8}{3\pi}\right)d_0\right] \tag{4}$$

where the second term inside the bracket in Eq. (3) has been ignored as $(9+X_0^2/2)^{-1/2} \ll 1$. The second term in Eq. (4), i.e. $(8/3\pi)d_0$ corresponds to the end correction at both ends of the hole, which is proportional to an added mass in the proximity of a moving piston [19]. This term will dominate for $d_0 \gg t$.

2.2. Mean particle velocity

In the presence of a distributed array of holes across the plate, the particle velocity at the plate surface is modified by the fluid flow through the holes v_f. The net particle velocity $\overline{v}$ formed by the combination of the normal velocity of the plate v and the fluid motion v_f is given by [12]

$$\overline{v} = v_p(1-\tau) + v_f \tag{5}$$

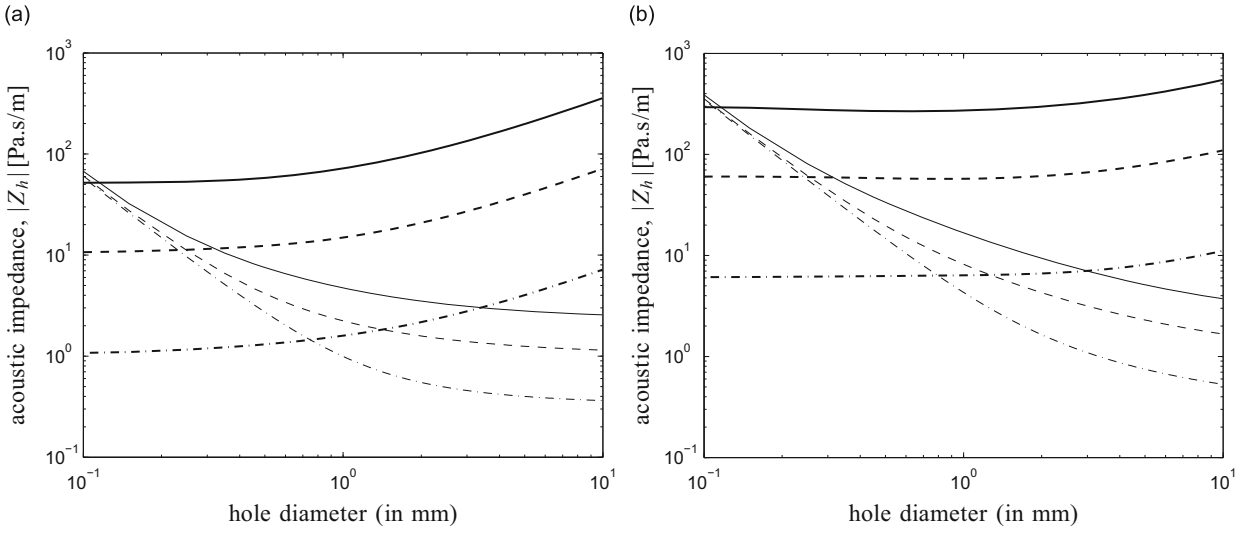

Fig. 1. The magnitude of the real (thin lines) and imaginary (thick lines) parts of the acoustic impedance of a circular hole in (a) 1 mm thick plate and (b) 6 mm thick plate (– · –100 Hz, – –1 kHz, —5 kHz).

where τ is the perforation ratio (proportion of the plate area which is open). For a continuous distribution of holes with perforation ratio τ, the equivalent fluid velocity through the holes averaged locally over the plate area will be $v_f = \tau v_h$ and the specific acoustic impedance of the distribution of holes will be $z_h = Z_h/\tau$. This can also be written as

$$z_h = \mathrm{j}\rho c h \tag{6}$$

where

$$h = \frac{k}{\tau}\left[t + \left(\frac{8}{3\pi}\right)d_0\right] \tag{7}$$

is the non-dimensional specific acoustic reactance, $k = \omega/c$ is the acoustic wavenumber and c is the speed of sound.

2.3. Baffled plate

2.3.1. Equally perforated baffle

Consider first a plane, harmonic bending wave of frequency ω and wavenumber k_x propagating in the x-direction in an infinite plate. The specific acoustic impedance presented to the upper surface of the plate by the fluid ($z > 0$), $z_a(k_x)$, is given by [4]

$$z_a(k_x) = \frac{P(k_x)}{V(k_x)} = \frac{\omega\rho}{(k^2 - k_x^2)^{1/2}}, \quad |k_x| \le k \tag{8}$$

where P and V are the complex acoustic pressure and complex plate velocity amplitudes, respectively. For $|k_x| > k$, $z_a(k_x)$ is imaginary (reactive) and a near-field is produced. Thus only $|k_x| \le k$ is considered here to calculate the propagating waves producing sound radiation.

For the case of a perforated plate, as shown in Fig. 2(a), following the method of [2] the difference between the local pressures on the upper and lower surfaces of the plate drives fluid through the individual holes. In turn, these pressures are modified by the flow through the holes. By symmetry, the pressure difference is $\Delta p = -2p$. Considering the holes as a continuous distribution, the equivalent fluid particle velocity $v_f(x)$, due to the flow through the holes can be given by

$$v_f(x) = \frac{-2p(x)}{z_h} \tag{9}$$

Therefore the mean particle velocity $\overline{v}$ as in Eq. (5) can be written as

$$\overline{v}(x) = v(x)(1-\tau) - \frac{2p(x)}{z_h} \tag{10}$$

Since the plate is assumed infinite and the bending wave has a unique wavenumber k_x, the plate and the equivalent fluid particle velocity also have the same unique wavenumber in the x direction. Eq. (10) can thus be expressed as

$$\overline{V}(k_x) = V(k_x)(1-\tau) - \frac{2P(k_x)}{z_h} \tag{11}$$

For the case of a finite perforated plate, Eq. (11) can still be applied provided that the rigid baffle shares the same impedance, i.e. it must also be constructed with the same degree of perforation as the plate, as indicated in Fig. 2(b). From here, using Eq. (8), the pressure P generated above the finite plate is

$$P(k_x) = \overline{V}(k_x) z_a(k_x) = \left(V(k_x)(1-\tau) - \frac{2P(k_x)}{z_h}\right) z_a(k_x) \tag{12}$$

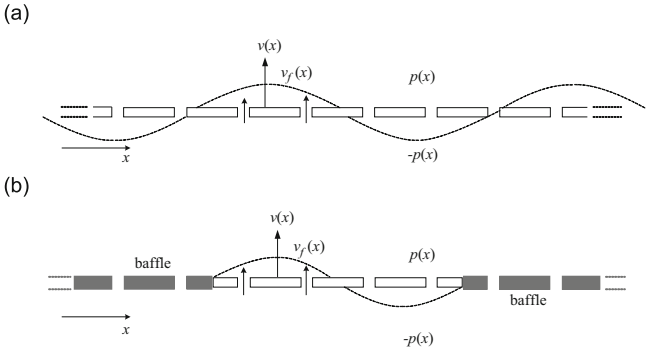

Fig. 2. Analytical model of a perforated plate: (a) an infinite perforated plate and (b) a perforated plate set in an equally perforated baffle.

Rearranging yields

$$P(k_x) = \frac{z_h z_a(k_x)(1-\tau)}{z_h + 2z_a(k_x)} V(k_x) \tag{13}$$

If the perforated panel is embedded in a solid rigid baffle (without perforation), then this will lead to a mixed boundary impedance, see [2], for which Eq. (12) can no longer be applied.

Finally substituting Eq. (13) into Eq. (11) yields the ratio of the complex amplitudes of the combined normal velocity of the plate and fluid flow through the holes (mean velocity) to that of the plate alone

$$\frac{\overline{V}(k_x)}{V(k_x)} = \frac{1-\tau}{1+2z_a(k_x)/z_h} \tag{14}$$

Eq. (14) confirms that the sound radiation from the plate is reduced by introducing perforation to the plate. As $|z_a(k_x)/z_h| \to \infty$, i.e. open area condition (absence of the plate), the ratio tends to zero so that flow through the holes completely compensates the plate motion, while as $z_a(k_x)/z_h \to 0$, i.e. the unperforated plate (absence of the holes), the ratio tends to unity. The sound power radiated per unit area of the perforated plate can be calculated from

$$W_p(k_x) = \tfrac{1}{2}\Re\{P(k_x)\overline{V}^*(k_x)\} \tag{15}$$

where * denotes the complex conjugate and $\Re$ indicates the real part. By using the relation from Eq. (8) this yields

$$W_p(k_x) = \tfrac{1}{2}\,\Re\{z_a(k_x)\overline{V}(k_x)\overline{V}^*(k_x)\} = \tfrac{1}{2}|\overline{V}(k_x)|^2\,\Re\{z_a(k_x)\} \tag{16}$$

The ratio of sound power per unit area of the perforated plate to that of the unperforated plate is therefore given by

$$\frac{W_p(k_x)}{W(k_x)} = \left|\frac{\overline{V}(k_x)}{V(k_x)}\right|^2 = \frac{1}{1+4(z_a(k_x)/|z_h|)^2} = \frac{h^2(1-(k_x/k)^2)(1-\tau)^2}{4+h^2(1-(k_x/k)^2)}, \quad |k_x| \le k \tag{17}$$

since z_h is imaginary and z_a is real.

For a plane wave travelling with components in the x and y directions, k_x^2 can be replaced by the square of the resultant, $k_x^2+k_y^2$. In terms of non-dimensional wavenumbers, it follows that Eq. (17) can therefore be written as

$$|X(\alpha,\beta)|^2 = \frac{h^2(1-\alpha^2-\beta^2)(1-\tau)^2}{4+h^2(1-\alpha^2-\beta^2)}, \quad \alpha^2+\beta^2 \le 1 \tag{18}$$

where $\alpha = k_x/k$ and $\beta = k_y/k$.

2.3.2. The acoustic sound power and radiation efficiency in terms of modal summation

From Eq. (17), the sound power from the perforated plate can be obtained from the sound power radiated by the solid plate. The plate velocity can be considered as the summation of plate modes (m,n) which can be written as

$$v(x,y) = \sum_{m=1}^{\infty}\sum_{n=1}^{\infty} u_{mn}\varphi_{mn}(x,y) \tag{19}$$

where u_{mn} is the modal complex velocity amplitude and φ_{mn} is the mode shape function. For the case of a simply supported plate with dimensions $a \times b$, the mode shape φ_{mn} is the product of two sinusoidal functions, i.e.

$$\varphi_{mn}(x,y) = \sin\left(\frac{m\pi x}{a}\right)\sin\left(\frac{n\pi y}{b}\right) \tag{20}$$

Here it is assumed that the individual modes are uniformly excited simultaneously and each mode acts as an independent energy reservoir [21].

The normal velocity distribution for each mode can be decomposed into a continuous spectrum of spatially harmonic, travelling plane wave components, each having a certain wavenumber vector given by

$$\tilde{V}_{mn}(k_x,k_y) = \int_0^a\int_0^b u_{mn}\varphi_{mn}\mathrm{e}^{-\mathrm{j}(k_x x+k_y y)}\,\mathrm{d}x\,\mathrm{d}y = u_{mn}\tilde{\varphi}_{mn}(k_x,k_y) \tag{21}$$

where $\tilde{\varphi}_{mn}$ is the Fourier transform of mode shape φ_{mn} given by

$$\tilde{\varphi}_{mn}(k_x,k_y) = \frac{ab}{\pi^2 mn}\left[\frac{(-1)^m\mathrm{e}^{-\mathrm{j}\mu}-1}{(\mu/(m\pi))^2-1}\right]\left[\frac{(-1)^n\mathrm{e}^{-\mathrm{j}\chi}-1}{(\chi/(n\pi))^2-1}\right] \tag{22}$$

with $\mu = k_x a$, $\chi = k_y b$.

From Eqs. (8) and (16) (for a travelling wave with components in the x and y directions), the sound power radiated by a mode of a plate can be obtained from integration over wavenumbers ranging from $-k$ to k, given by [4]

$$W_{mn} = \frac{\rho c}{8\pi^2}\int_{-k}^{k}\int_{-\sqrt{k^2-k_y^2}}^{\sqrt{k^2-k_y^2}} \frac{k}{(k^2-k_x^2-k_y^2)^{1/2}}|\tilde{V}_{mn}(k_x,k_y)|^2\,\mathrm{d}k_x\,\mathrm{d}k_y \tag{23}$$

Note that only wavenumber components satisfying the condition $k_x^2+k_y^2 \le k^2$ and therefore contributing to sound power radiation have been considered. Using Eqs. (17) and (18) and by substituting Eq. (21), the sound power from a mode of a perforated plate in terms of non-dimensional wavenumbers (α,β) can be expressed as

$$W_{mn} = \frac{\rho c |u_{mn}|^2}{8\pi^2} \int_{-1}^{1} \int_{-\sqrt{1-\beta^2}}^{\sqrt{1-\beta^2}} |X(\alpha,\beta)|^2 \frac{|\tilde{\varphi}_{mn}(\alpha,\beta)|^2}{(1-\alpha^2-\beta^2)^{1/2}} \, \mathrm{d}\alpha \, \mathrm{d}\beta \tag{24}$$

where $\tilde{\varphi}_{mn}$ can be written in terms of $\mu = \alpha ka$ and $\chi = \beta kb$. The modal radiation efficiency can be calculated from

$$\sigma_{mn} = \frac{W_{mn}}{\frac{1}{2}\rho c (1-\tau) S \overline{\langle |v_{mn}|^2 \rangle}} \tag{25}$$

where $\overline{\langle |v_{mn}|^2 \rangle}$ is the spatially averaged squared velocity amplitude in mode (m,n) and $S=ab$ is the total plate area. This has been averaged over all possible force positions. This is derived from the spatially averaged squared velocity distribution of a mode expressed as

$$\langle |v_{mn}|^2 \rangle = \frac{1}{S} \int_S |v_{mn}(x,y)|^2 \, \mathrm{d}x \, \mathrm{d}y \tag{26}$$

After averaging over all possible forcing locations (x_0,y_0)

$$\overline{\langle |v_{mn}|^2 \rangle} = \frac{1}{ab} \int_0^a \int_0^b \langle |v_{mn}|^2 \rangle \, \mathrm{d}x_0 \, \mathrm{d}y_0 \tag{27}$$

Substituting Eq. (19) for each mode for a simply supported plate yields

$$\overline{\langle |v_{mn}|^2 \rangle} = \frac{|u_{mn}|^2}{4} \tag{28}$$

In Eq. (25), the spatially averaged squared velocity has been multiplied by $(1-\tau)S$, i.e. the solid area of the perforate which radiates sound into the air. The term $(1-\tau)$, however, only has significant effect for high perforation ratio. Substituting Eqs. (24) and (28) into Eq. (25), the modal radiation efficiency of a perforated plate set in an equally perforated baffle is given by

$$\sigma_{mn} = \frac{1}{(1-\tau)S\pi^2} \int_{-1}^{1} \int_{-\sqrt{1-\beta^2}}^{\sqrt{1-\beta^2}} |X(\alpha,\beta)|^2 \frac{|\tilde{\varphi}_{mn}(\alpha,\beta)|^2}{(1-\alpha^2-\beta^2)^{1/2}} \, \mathrm{d}\alpha \, \mathrm{d}\beta \tag{29}$$

The total radiation efficiency σ can be defined as a summation over the contributions of all modes [22]

$$\sigma = \frac{\sum_{m=1}^{\infty} \sum_{n=1}^{\infty} W_{mn}}{\rho c (1-\tau) S \sum_{m=1}^{\infty} \sum_{n=1}^{\infty} \overline{\langle |v_{mn}|^2 \rangle}} = \frac{\sum_{m=1}^{\infty} \sum_{n=1}^{\infty} \sigma_{mn} [(\omega_{mn}^2-\omega^2)^2+\eta^2\omega_{mn}^4]^{-1}}{\sum_{m=1}^{\infty} \sum_{n=1}^{\infty} [(\omega_{mn}^2-\omega^2)^2+\eta^2\omega_{mn}^4]^{-1}} \tag{30}$$

where η is the damping loss factor and $\omega_{mn} = (B/\rho_s t)^{1/2}[(m\pi/a)^2+(n\pi/b)^2]$ is the natural frequency with ρ_s the plate density and $B = Et^3/12(1-v^2)$ the plate bending stiffness in which E is Young's modulus and v is Poisson's ratio.

2.4. Unbaffled plate

2.4.1. Governing fundamental equations

Considering now an unbaffled perforated plate, Laulagnet's model [10] for the sound radiation from an unbaffled plate is extended to include perforation. Fig. 3 shows a flat thin perforated unbaffled plate with a surface area S located in an infinite medium. The plate is excited by a harmonic force distribution $F(x,y)$ of angular frequency ω. $\Delta p(x,y)$ is the difference between the acoustic surface pressure on the two sides of the plate defined as

$$\Delta p(x,y) = p^-(x,y) - p^+(x,y) \tag{31}$$

The equation of motion of a perforated plate with a perforation ratio τ excited by the force distribution F and pressure difference Δp is

$$\frac{B}{\mathrm{j}\omega} \nabla^4 v(x,y) + \mathrm{j} m_s \omega v(x,y) = F(x,y) + (1-\tau)\Delta p(x,y) \tag{32}$$

where B is the bending stiffness, $m_s = \rho_s t$ is the mass per unit area, $v(x,y)$ is the transverse velocity of the plate and $\nabla^4 = \partial^4/\partial x^4 + 2\partial^4/(\partial x^2 \partial y^2) + \partial^4/\partial y^4$. The bending stiffness and mass per unit area also depend on the extent of perforation but this is neglected here.

The pressure at a point M in the fluid can be defined by using the Kirchhoff–Helmholtz (K–H) integral

$$p(M) = \int_{S_v} \left(p(Q) \frac{\partial G(Q,M)}{\partial n_Q} - G(Q,M) \frac{\partial p}{\partial n_Q} \right) \mathrm{d}S_v \tag{33}$$

where Q is a point on the plate surface, G is the free-field Green's function and S_v is the surface area of the volume enclosing the plate. Therefore the integral is performed over both sides of the plate (the integral over the surface at infinity can be

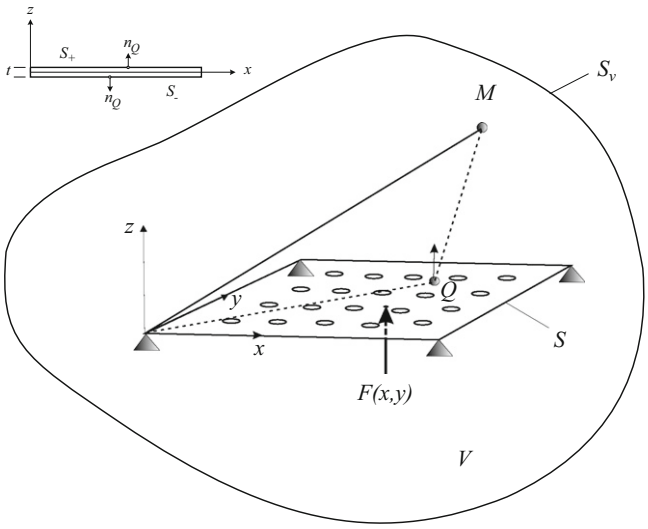

Fig. 3. A simply supported perforated plate enclosed by a volume V in the medium with its bounding surface S_v.

neglected). In Eq. (33), the first and second terms correspond to the dipole and monopole source radiation, respectively. By using the two dimensional spatial Fourier transform, the Green's function can be expressed as [23]

$$G = \frac{\mathrm{j}}{8\pi^2}\int_{-\infty}^{\infty}\int_{-\infty}^{\infty}\frac{\mathrm{e}^{\mathrm{j}k_x(x-x_0)}\mathrm{e}^{\mathrm{j}k_y(y-y_0)}\mathrm{e}^{\mathrm{j}k_z(z-z_0)}}{k_z}\mathrm{d}k_x\,\mathrm{d}k_y \tag{34}$$

where $k_z=(k^2-k_x^2-k_y^2)^{1/2}$, $Q=(x,y,z)$ is a point on the plate surface ($z=0$), $M=(x_0,y_0,z_0)$ is a field point and attention is limited to the pressure at a point M above the plate (in the half-space $z_0\geq 0$).

Since the plate thickness is assumed to be very small, the normal velocity is identical on the plate surfaces S_+ and S_- and hence $\partial p/\partial z_Q$ is equal on both sides of the plate. However the sign of the normal vector $\mathbf{n}_Q$ is reversed so that the second term in Eq. (33) is zero. Thus by performing the integration over the plate surface, Eq. (33) reduces to

$$p(M)|_{z=0} = -\int_S \Delta p\frac{\partial G(Q,M)}{\partial z_Q}\,\mathrm{d}S \tag{35}$$

leaving only the dipole term.

For the case of a vibrating perforated plate, applying Euler's equation to Eq. (35) in the plane of the plate at $z=0$ gives

$$\left.\frac{\partial p}{\partial z}(M)\right|_{z=0} = -\mathrm{j}\rho\omega\overline{v}(M) \tag{36}$$

Substituting Eq. (5)

$$\left.\frac{\partial p}{\partial z}(M)\right|_{z=0} = -\mathrm{j}\rho\omega(v(M)(1-\tau)+v_f(M)) = -\mathrm{j}\rho\omega(1-\tau)v(M)-\frac{\mathrm{j}\rho\omega}{z_h}\Delta p(M) \tag{37}$$

where, as in Section 2.3, v is the velocity of the plate and v_f is the locally averaged fluid motion. Substituting Eq. (32) into Eq. (37) to eliminate the pressure difference Δp yields

$$\left.\frac{\partial p}{\partial z}(M)\right|_{z=0} = -\mathrm{j}\rho\omega(1-\tau)v(M)-\frac{\mathrm{j}\rho\omega}{z_h(1-\tau)}\left(\frac{B}{\mathrm{j}\omega}\nabla^4 v(x,y)+\mathrm{j}m_s\omega v(x,y)-F(x,y)\right) \tag{38}$$

Substituting this into Eq. (35)

$$-\mathrm{j}\rho\omega(1-\tau)^2 v(M)-\frac{\mathrm{j}\rho\omega}{z_h}\left(\frac{B}{\mathrm{j}\omega}\nabla^4 v(M)+\mathrm{j}m_s\omega v(M)-F(M)\right) = -\int_S\left(\frac{B}{\mathrm{j}\omega}\nabla^4 v(Q)+\mathrm{j}m_s\omega v(Q)-F(Q)\right)\frac{\partial^2 G(Q,M)}{\partial z_Q\partial z_M}\mathrm{d}S \tag{39}$$

where, compared with [10], the second term on the left-hand side has been introduced by the perforation.

2.4.2. Force excitation in terms of modal series

The plate velocity can again be considered as the summation of plate modes (m,n) as given in Eq. (19). The same is also applied to the excitation force F which is written as

$$F(x,y) = \sum_{m=1}^{\infty}\sum_{n=1}^{\infty} F_{mn}\varphi_{mn}(x,y) \tag{40}$$

where F_{mn} is the modal force amplitude and φ_{mn} is the mode shape function. As in Section 2.3, the modal force F_{mn} is also assumed to produce equal excitation energy in each mode. Using Eq. (20) it is obtained that

$$\nabla^4\varphi_{mn}(x,y)=\left(\frac{m_s\omega_{mn}^2}{B}\right)\varphi_{mn}(x,y) \tag{41}$$

The effect of damping can be included by replacing the plate bending stiffness B by $B(1+j\eta)$. The orthogonality relationship with mode (p,q) for a simply supported uniform plate gives

$$\int_S \varphi_{mn}\varphi_{pq}\,\mathrm{d}S=\frac{S}{4}\delta_{mp}\delta_{nq} \tag{42}$$

Writing in terms of the modal series of velocity v and excitation force F, Eq. (39) can be expressed as

$$\begin{aligned}-\mathrm{j}\rho\omega(1-\tau)^2\sum_{m=1}^{\infty}\sum_{n=1}^{\infty}u_{mn}\varphi_{mn}(x_0,y_0)-\frac{\mathrm{j}\rho\omega}{z_h}\sum_{m=1}^{\infty}\sum_{n=1}^{\infty}\left(\frac{B}{\mathrm{j}\omega}u_{mn}\nabla^4\varphi_{mn}(x_0,y_0)+\mathrm{j}m_s\omega u_{mn}\varphi_{mn}(x_0,y_0)-F_{mn}\varphi_{mn}(x_0,y_0)\right)\\ =-\int_S\sum_{m=1}^{\infty}\sum_{n=1}^{\infty}\left(\frac{B}{\mathrm{j}\omega}u_{mn}\nabla^4\varphi_{mn}(x,y)+\mathrm{j}m_s\omega u_{mn}\varphi_{mn}(x,y)-F_{mn}\varphi_{mn}(x,y)\right)\frac{\partial^2G(Q,M)}{\partial z_Q\partial z_M}\,\mathrm{d}S\end{aligned} \tag{43}$$

Substituting Eq. (41) to eliminate the terms $\nabla^4\varphi_{mn}$ yields

$$\begin{aligned}(1-\tau)^2\rho\omega^2\sum_{m=1}^{\infty}\sum_{n=1}^{\infty}u_{mn}\varphi_{mn}(x_0,y_0)-\frac{\mathrm{j}\rho\omega}{z_h}\sum_{m=1}^{\infty}\sum_{n=1}^{\infty}(m_s(\omega_{mn}^2-\omega^2)u_{mn}-\mathrm{j}\omega F_{mn})\varphi_{mn}(x_0,y_0)\\ =-\int_S\sum_{m=1}^{\infty}\sum_{n=1}^{\infty}(m_s(\omega_{mn}^2-\omega^2)u_{mn}-\mathrm{j}\omega F_{mn})\varphi_{mn}(x,y)\frac{\partial^2G(Q,M)}{\partial z_Q\partial z_M}\,\mathrm{d}S\end{aligned} \tag{44}$$

2.4.3. Acoustic cross-modal coupling terms

Using Eq. (42), after multiplying Eq. (44) by φ_{pq} and integrating over the plate area

$$(1-\tau)^2\rho\omega^2\left(\frac{S}{4}\right)u_{pq}-\frac{\mathrm{j}\rho\omega}{z_h}\left(\frac{S}{4}\right)(m_s(\omega_{pq}^2-\omega^2)u_{pq}-\mathrm{j}\omega F_{pq})=\sum_{m=1}^{\infty}\sum_{n=1}^{\infty}(\mathrm{j}\omega F_{mn}-m_s(\omega_{mn}^2-\omega^2)u_{mn})C_{pqmn} \tag{45}$$

where

$$C_{pqmn}=\int_S\int_S\varphi_{pq}(x_0,y_0)\frac{\partial^2G}{\partial z\partial z_0}(x,x_0,y,y_0,z=z_0=0)\varphi_{mn}(x,y)\,\mathrm{d}x\,\mathrm{d}y\,\mathrm{d}x_0\,\mathrm{d}y_0 \tag{46}$$

Substituting Eq. (34) into Eq. (46) and performing the two integrals over S yields

$$C_{pqmn}=\frac{\mathrm{j}}{8\pi^2}\int_{-\infty}^{\infty}\int_{-\infty}^{\infty}k_z\tilde{\varphi}_{pq}^*(k_x,k_y)\tilde{\varphi}_{mn}(k_x,k_y)\,\mathrm{d}k_x\,\mathrm{d}k_y \tag{47}$$

where $\tilde{\varphi}_{mn}$ is the Fourier transform of mode shape φ_{mn} given as in Eq. (22). After algebraic manipulation, for simply supported edges, Eq. (47) can be expressed as

$$C_{pqmn}=\frac{2j}{pqmn}\left(\frac{ab}{\pi^3}\right)^2\int_0^{\infty}\int_0^{\infty}k_z\,\Upsilon\Omega\,\mathrm{d}k_x\,\mathrm{d}k_y \tag{48}$$

where

$$\Upsilon=\frac{1-(-1)^p\cos\mu}{((\mu/p\pi)^2-1)((\mu/m\pi)^2-1)},\quad \Omega=\frac{1-(-1)^q\cos\chi}{((\chi/q\pi)^2-1)((\chi/n\pi)^2-1)} \tag{49}$$

with $\mu=k_xa$, $\chi=k_yb$. The lower limit of integration has been changed from $-\infty$ to 0 because the integrand, with respect to k_x, is an even function when the mode orders (p,m) are of the same parity. Similarly, with respect to k_y, it is an even function when the mode orders (q,n) are of the same parity. The remaining cases will have C_{pqmn}=0. After re-arranging Eq. (45), it can be written in matrix form as

$$\begin{aligned}m_s\mathbf{C}(\mathbf{A}-\mathbf{I}\omega^2)\mathbf{u}+(1-\tau)^2\rho\omega^2\left(\frac{S}{4}\right)\mathbf{u}-\frac{\mathrm{j}\rho\omega m_s}{z_h}\left(\frac{S}{4}\right)(\mathbf{A}-\mathbf{I}\omega^2)\mathbf{u}\\ =\mathrm{j}\omega\mathbf{C}\mathbf{F}+\frac{\rho\omega^2}{z_h}\left(\frac{S}{4}\right)\mathbf{F}\end{aligned} \tag{50}$$

where $\mathbf{C}$ is the matrix of complex acoustic coupling terms C_{pqmn}, $\mathbf{u}$ is the vector of modal velocities u_{mn}, $\mathbf{F}$ is the vector of modal excitation forces F_{mn}, $\mathbf{I}$ is the identity matrix and $\mathbf{A}$ is a diagonal matrix of squared natural frequencies

$$\mathbf{A}=\begin{bmatrix}\omega_{11}^2 & 0 & \cdots & 0\\ 0 & \omega_{12}^2 & \cdots & \vdots\\ \vdots & \vdots & \ddots & \vdots\\ 0 & \cdots & \cdots & \omega_{mn}^2\end{bmatrix} \tag{51}$$

Multiplying Eq. (50) by $\mathbf{C}^{-1}$, i.e. the inverse of matrix $\mathbf{C}$ yields

$$m_s(\mathbf{A}-\mathbf{I}\omega^2)\mathbf{u}+\rho\omega^2\left(\frac{S}{4}\right)\mathbf{C}^{-1}\left((1-\tau)^2\mathbf{I}-\frac{\mathrm{j}m_s}{\omega z_h}(\mathbf{A}-\mathbf{I}\omega^2)\right)\mathbf{u}=\left(\mathrm{j}\omega\mathbf{I}+\frac{\rho\omega^2}{z_h}\left(\frac{S}{4}\right)\mathbf{C}^{-1}\right)\mathbf{F} \tag{52}$$

Eq. (52) can be simplified by taking only the self-modal coupling terms of Eq. (48). The inverse of the cross-modal coupling terms $\mathbf{C}^{-1}$ can then be replaced by a diagonal matrix of terms $1/C_{pqpq}$. Such an approximation works well for a baffled plate [24], particularly when the average result over different force positions is considered [22]. It has been shown that this approximation can also be used for the case of an unbaffled plate immersed in a light fluid such as air. For a heavy fluid loading such as water, the off-diagonal terms become important, particularly for the radiated sound power [10].

By neglecting the cross-modal coupling contributions in the sound radiation, this can be approximated by

$$M_{pq}(\omega_{pq}^2-\omega^2)u_{pq}+\rho\omega^2\left(\frac{S}{4}\right)^2\left(\frac{1}{C_{pqpq}}\right)\left((1-\tau)^2-\frac{4\mathrm{j}M_{pq}}{S\omega z_h}(\omega_{pq}^2-\omega^2)\right)u_{pq}=\left(\mathrm{j}\omega+\frac{\rho\omega^2}{z_h}\left(\frac{S}{4}\right)\frac{1}{C_{pqpq}}\right)\left(\frac{S}{4}\right)F_{pq} \tag{53}$$

where $M_{pq}=m_s(S/4)$ is the generalized mass for mode (p,q). The case of the unperforated (solid) unbaffled plate, as in [10], can be recovered by introducing very large z_h and setting $\tau=0$.

Eq. (53) can be solved to find the modal complex velocity amplitude u_{pq}. From this, the spatially averaged squared velocity amplitude of a plate mode $\langle|v_{pq}|^2\rangle$ is obtained (see Eq. (28)).

2.4.4. The acoustic sound power and radiation efficiency in terms of modal summation

The acoustic pressure is determined from the pressure difference $\Delta p(x,y)$ between the two sides of the plate surface. The normal vector $\mathbf{n}$ is pointing away from the plate as seen in Fig. 3. Therefore the total radiated sound power from both sides of the plate can be defined as

$$\begin{aligned}W&=\frac{1}{2}\int_S\Re\left\{\sum_{p=1}^{\infty}\sum_{q=1}^{\infty}p_+(x,y)\mathbf{v}_{pq}^*(x,y)\cdot\mathbf{n}\,\mathrm{d}S_+ + p_-(x,y)\mathbf{v}_{pq}^*(x,y)\cdot\mathbf{n}\,\mathrm{d}S_-\right\}\\&=-\frac{1}{2}\int_S\Re\left\{\sum_{p=1}^{\infty}\sum_{q=1}^{\infty}\Delta p(x,y)v_{pq}^*(x,y)\right\}\mathrm{d}S\end{aligned} \tag{54}$$

where * denotes complex conjugate.

To obtain a convenient calculation, the pressure difference $\Delta p(x,y)$ can also be written in terms of a series of plate modes [10]

$$\Delta p(x,y)=\sum_{m=1}^{\infty}\sum_{n=1}^{\infty}p_{mn}\varphi_{mn}(x,y) \tag{55}$$

where p_{mn} are the corresponding amplitudes. Therefore by using the orthogonality relationship from Eq. (42), the radiated sound power can be written as

$$W=-\frac{1}{2}\int_S\Re\left\{\sum_{m=1}^{\infty}\sum_{n=1}^{\infty}p_{mn}\varphi_{mn}\times\sum_{p=1}^{\infty}\sum_{q=1}^{\infty}u_{pq}^*\varphi_{pq}\right\}\mathrm{d}S=-\frac{1}{2}\left(\frac{S}{4}\right)\Re\left\{\sum_{p=1}^{\infty}\sum_{q=1}^{\infty}p_{pq}u_{pq}^*\right\} \tag{56}$$

To find p_{pq}, Eq. (32) can be used with Eqs. (41) and (55) to give

$$\sum_{m=1}^{\infty}\sum_{n=1}^{\infty}m_s(\omega_{mn}^2-\omega^2)u_{mn}\varphi_{mn}(x,y)=\mathrm{j}\omega\sum_{m=1}^{\infty}\sum_{n=1}^{\infty}F_{mn}\varphi_{mn}(x,y)+\mathrm{j}\omega(1-\tau)\sum_{m=1}^{\infty}\sum_{n=1}^{\infty}p_{mn}\varphi_{mn}(x,y) \tag{57}$$

Again, applying the orthogonality relationship (Eq. (42)) yields

$$m_s(\omega_{pq}^2-\omega^2)u_{pq}=\mathrm{j}\omega(F_{pq}+(1-\tau)p_{pq}) \tag{58}$$

which allows p_{pq} to be found. The radiated power for each mode can be obtained by substituting p_{pq} from Eq. (58) into Eq. (56)

$$W_{pq}=\frac{S}{8(1-\tau)}\Re\{(F_{pq}-m_s(\omega_{pq}^2-\omega^2)u_{pq}/\mathrm{j}\omega)u_{pq}^*\} \tag{59}$$

The total radiation efficiency can be calculated using Eq. (30).

The radiation efficiency of the unbaffled plate takes into account the fluid loading on both sides of the plate. Therefore the total surface area of the plate $S=2ab$ should be used in Eq. (30).

3. Results

3.1. Radiation efficiency results

Fig. 4 shows the radiation efficiencies of baffled and unbaffled solid (unperforated) plates. These are obtained by setting a very high value of z_h and $\tau=0$ in both models. These results are for an example aluminium plate of dimensions $0.65\times0.5\times0.003$ m with $\eta=0.1$, excited by a unit point force and represents the average over force positions over the plate surface.

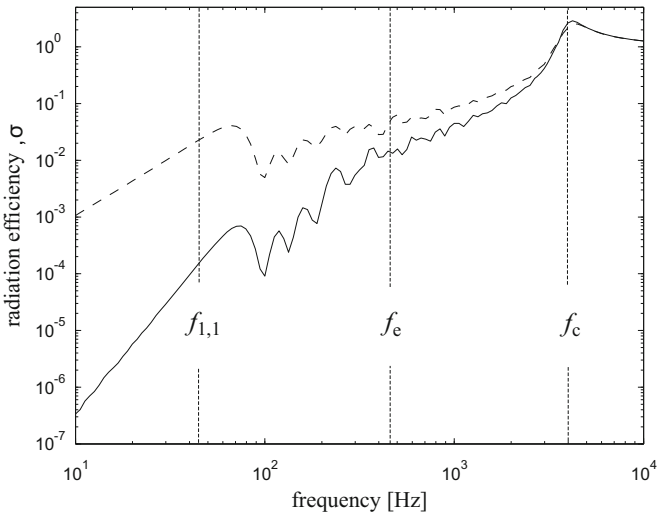

Fig. 4. Radiation efficiency of a simply supported baffled (−−) and unbaffled (—) plate (0.65 × 0.5 × 0.003 m aluminium plate with $\eta = 0.1$).

The calculation is made up to 10 kHz involving all modes with $m \leq 25$ and $n \leq 20$. The material properties are taken as $E = 7.1 \times 10^{10}\,\mathrm{N/m^2}$, $\rho_s = 2700\,\mathrm{kg/m^3}$, $\nu = 0.33$.

To help interpret these results, the frequency region can be divided into the fundamental mode region, below the first plate resonance frequency $f_{1,1}$, the corner mode region between $f_{1,1}$ and the frequency f_e given by [4,25]

$$f_e = \frac{3c}{P} \tag{60}$$

where $P = 2(a+b)$ is the plate perimeter, the edge mode region between f_e and the critical frequency f_c,

$$f_c = \frac{c^2}{2\pi}\left(\frac{\rho_s t}{B}\right)^{1/2} \tag{61}$$

and the supersonic region above f_c.

The two results show different levels and trends of the radiation efficiency. The slopes at very low frequency, i.e. below the first resonance frequency ($f_{1,1}$=46 Hz) are 20 and 40 dB/decade, showing the characteristic of monopole and dipole source radiation for baffled and unbaffled plates, respectively. In the corner mode region between $f_{1,1}$ and f_e, the result increases by roughly 10 dB/decade for the baffled case and 30 dB/decade for the unbaffled case. Both curves increase above f_e in the edge mode region towards a peak at the critical frequency f_c=4 kHz. The whole plate surface then radiates sound effectively above the critical frequency (the supersonic region) where the radiation efficiency converges to unity $\sigma = 1$ at very high frequency.

In Fig. 5 the radiation efficiencies are shown for the same plate but with 5 percent perforation ratio and 5 mm diameter holes. Results are shown from both baffled and unbaffled models. The average radiation efficiency is plotted together with the modal radiation efficiencies in each case. It is interesting to note that the slope of the radiation efficiency for the baffled plate changes to 40 dB/decade below the first resonance frequency as shown in Fig. 5(a). This is due to the perforation of the baffle, which opens the 'communication' of the sound fields between the front and the back of the plate and provides cancellation of the monopole sources. For the unbaffled plate in Fig. 5(b), the trend of the slope is the same as for the solid plate in Fig. 4 except that there is a reduction in the radiation efficiency. It is also lower than that of the baffled plate in Fig. 5(a). It can be seen that for both cases the result at very low frequencies in the fundamental mode region is dominated by mode (1,1), which is also the case for the solid plate.

Results for other perforation ratios with 10 mm hole diameter are shown in Fig. 6, plotted in terms of the radiation index, $10\log_{10}\sigma$. This shows that the sound radiation is reduced as the perforation ratio is increased. As already mentioned, perforation gives a significant reduction in the case of a plate set in an equally perforated baffle particularly at very low frequency. At these frequencies, where the acoustic wavelength is greater than the plate dimensions, perforation of the baffle has a greater effect on the sound reduction than perforation of the plate itself. This is why a large reduction can be seen at low frequency where the plate exhibits behaviour that is closer to an unbaffled plate.

For the unbaffled plate, perforation leads to an almost constant reduction in radiation index for frequencies up to the corner mode region (which commences at 450 Hz in this case). For both cases, the perforation effect reduces as frequency increases. This can be expected as the impedance of the hole is proportional to frequency (see Eq. (4)). Therefore at high frequency, the fluid in the holes has a very high mass-like impedance. This mass does not move sufficiently to compensate for the volume sources adjacent to the hole. The cancellation of radiated sound thus becomes ineffective.

Fig. 7 shows the difference between the radiation index of baffled (σ_{bf}) and unbaffled (σ_{ubf}) perforated plates on a dB scale, i.e. $10\log_{10}(\sigma_{\mathrm{ubf}}/\sigma_{\mathrm{bf}})$. It is seen that the sound radiation for the plate in an equally perforated baffle is less than for

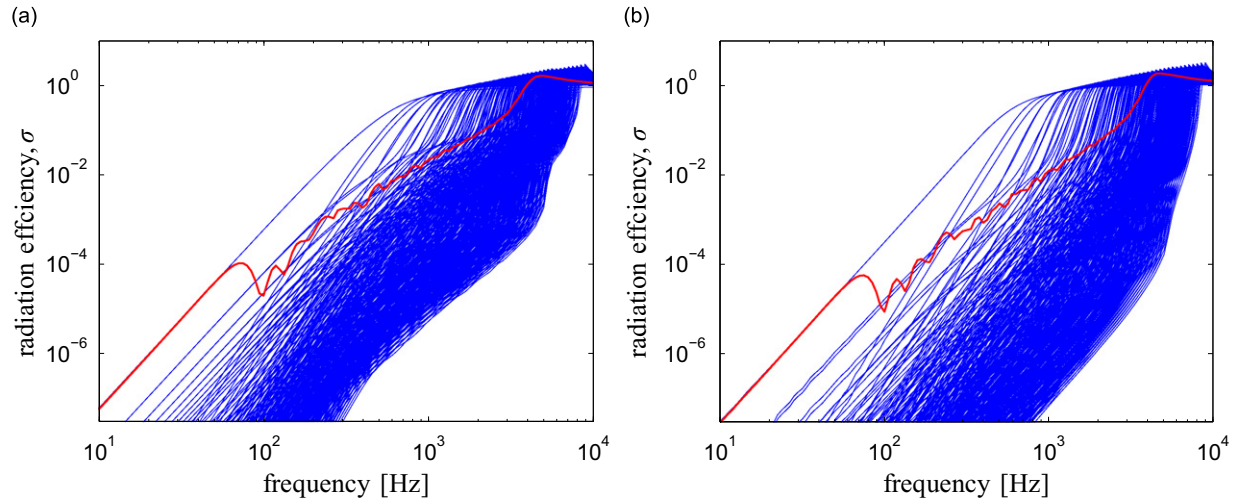

Fig. 5. Radiation efficiency of simply supported baffled (a) and unbaffled (b) perforated plates ($0.65 \times 0.5 \times 0.003$ m aluminium plate; d_0=5 mm, $\tau = 5$ percent): modal radiation efficiency (thin lines), radiation efficiency, $\eta = 0.1$ (thick line).

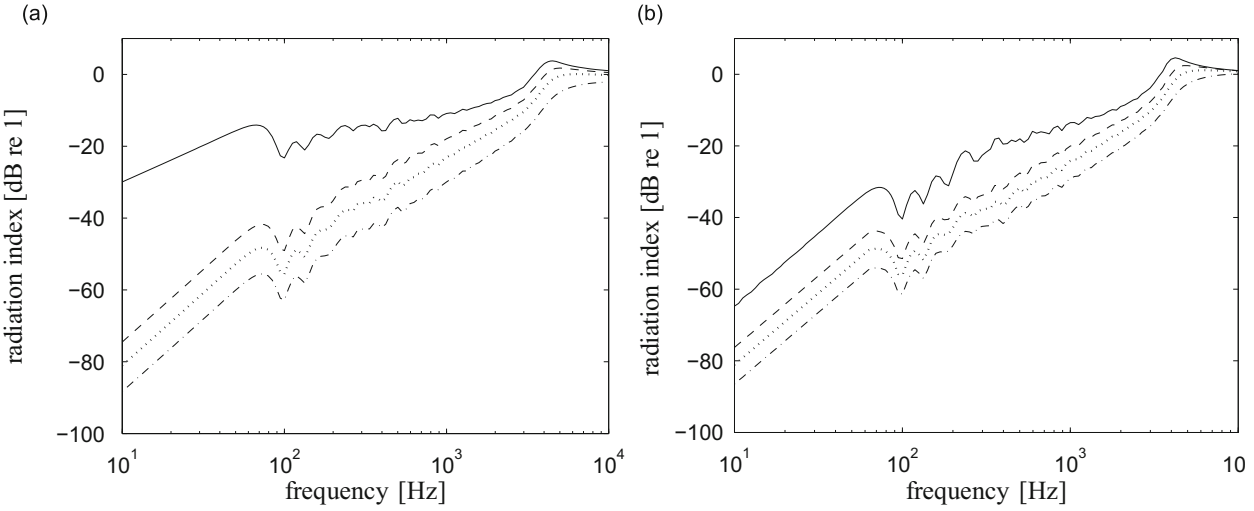

Fig. 6. Radiation index of simply supported baffled (a) and unbaffled (b) plates; d_0=10 mm: — solid, – – $\tau = 10$ percent, $\cdots$ $\tau = 20$ percent, – · – $\tau = 40$ percent ($0.65 \times 0.5 \times 0.003$ m aluminium plate with $\eta = 0.1$).

the unbaffled plate at very high perforation ratios (40 percent). However, for moderate perforation (20 percent), the difference is within ± 1.5 dB which shows that both models show similar results. For smaller perforation ratios the perforated baffle model gives an over-prediction of the radiation index relative to the unbaffled plate model as the perforation of the baffle is insufficient to allow full 'communication' between the two sides of the plate.

3.2. *Effect of perforation*

The reduction in sound level due to perforation can be defined in terms of the effect of perforation Θ, given by

$$\Theta = 10 \log_{10}\left(\frac{W_p}{W_s}\right) \tag{62}$$

where W_p and W_s are the radiated sound power for the perforated plate and solid or unperforated plate, respectively. This is related to the insertion loss (IL) commonly used in noise control by $\Theta = -\text{IL}$. For moderate perforation, where the term $1-\tau$ can be ignored, the effect of perforation on sound radiation can be approximated by the ratio of the radiation efficiencies of perforated (σ_p) and solid plates (σ_s), i.e. $\Theta = 10 \log_{10}(\sigma_p/\sigma_s)$. However, for large τ this is no longer correct.

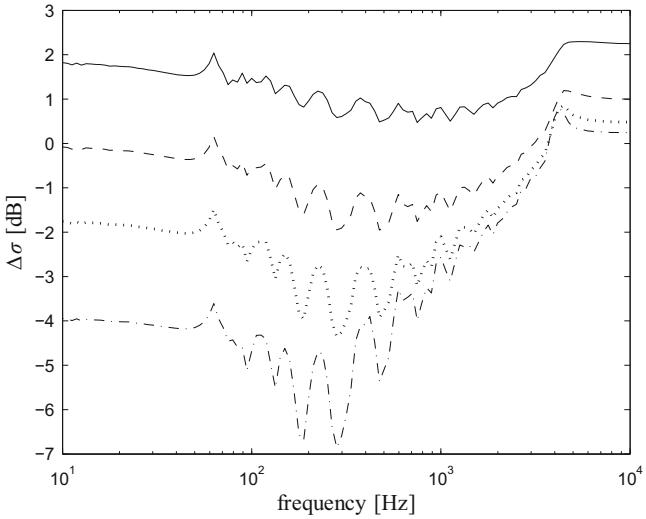

Fig. 7. Difference in radiation index of simply supported baffled and unbaffled perforated plates; d_0=10 mm: $-\cdot-\tau=5$ percent, $\cdots\tau=10$ percent, $--\tau=20$ percent, $—\tau=40$ percent (0.65 × 0.5 × 0.003 m aluminium plate with $\eta=0.1$).

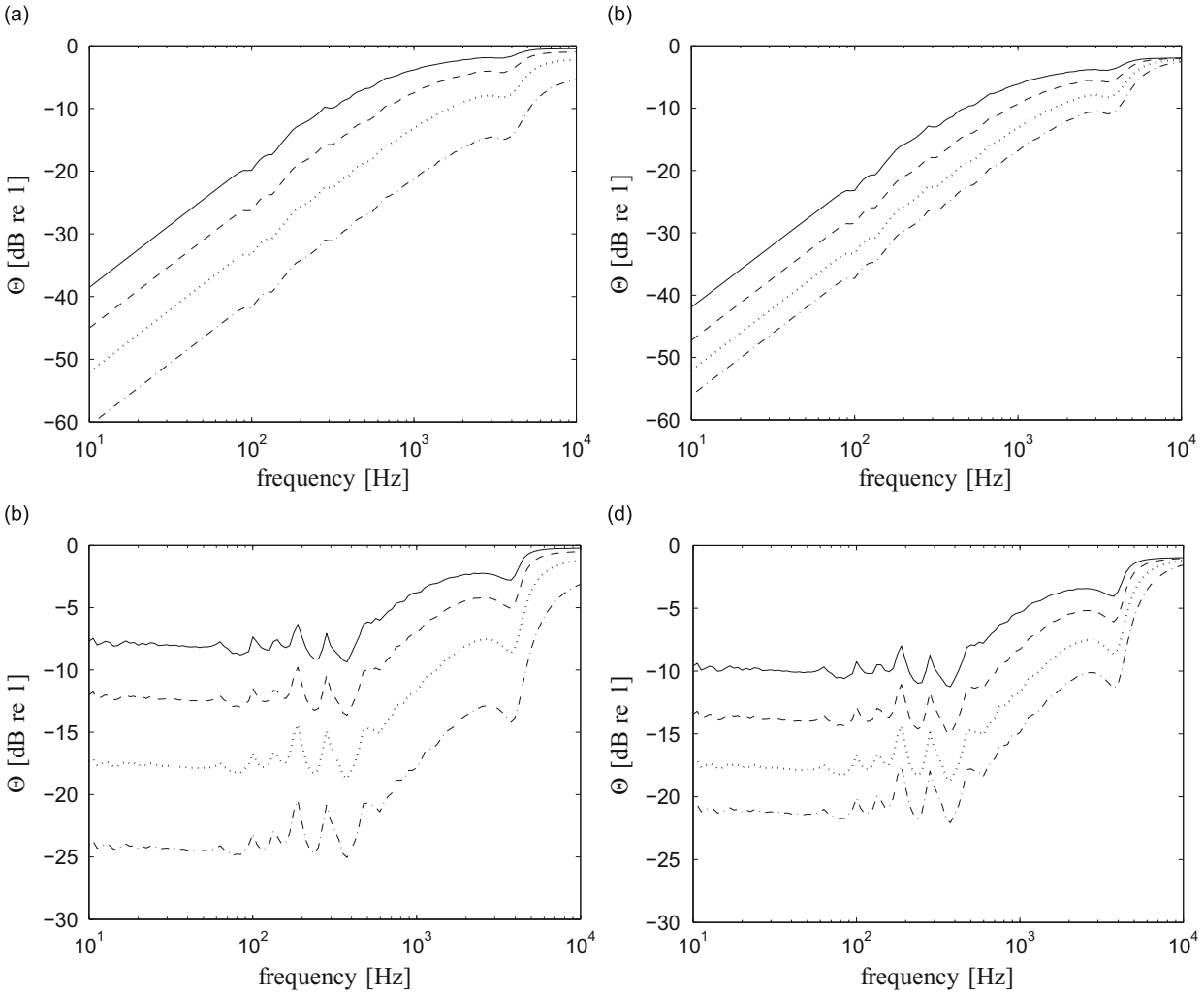

Fig. 8. Effect of perforation on sound power radiation of simply supported perforated baffled (a)–(b) and unbaffled (c)–(d) plates: (left) d_0=10 mm: $—\tau=5$ percent, $--\tau=10$ percent, $\cdots\ \tau=20$ percent, $-\cdot-\ \tau=40$ percent; (right) $\tau=20$ percent: — d_0= 40 mm, -- $d_0=20$ mm, $\cdots\ d_0=10$ mm, $-\cdot-\ d_0=5$ mm (0.65 × 0.5 × 0.003 m aluminium plate with $\eta=0.1$).

Fig. 8 presents the effect of perforation for constant hole diameter (left-hand side) and constant perforation ratio (right-hand side) for both models. It can be seen that below 450 Hz, both cases show different trends of the effect of perforation. Meanwhile above 450 Hz, the trend is almost similar. For the baffled perforated plate, due to the perforated baffle, the effect of perforation increases by 20 dB/decade at low frequency before approaching 0 dB at high frequency. For the case of the unbaffled perforated plate, the effect of perforation is almost independent of frequency in the fundamental and corner mode regions (<450 Hz) and then increases in the edge mode region as the frequency increases. The effect again approaches 0 dB at high frequency. Figs. 8(a) and (c) show that sound radiation is reduced by increasing the perforation ratio, while Figs. 8(b) and (d) show that for a constant perforation ratio, the radiated sound can be further reduced by reducing the hole size.

It can be seen from these results that the effect of perforation is reduced above the critical frequency, in this case 4 kHz. However, it does not tend to 0 at the critical frequency but can still be significant at higher frequencies than this.

From Eq. (7), for a plate where the plate thickness is much smaller than the hole radius, $t \ll d_0$, the non-dimensional specific acoustic reactance is dominated by the end correction and can be expressed as $h=(8k/3\pi)d_0/\tau$. Consequently, the effect of perforation is controlled by the factor d_0/τ. As seen from Fig. 8, for the same values of d_0/τ, the effect of the perforation is almost equal. For example d_0=10 mm, $\tau=10$ percent and d_0=20 mm, $\tau=20$ percent give similar results in each model (roughly 1.5 dB difference). However, the perforation ratio should not be too large as this will affect the area of the radiating surface.

4. Experimental validation

4.1. Experimental arrangement

Measurements have been conducted to determine the radiation efficiency of a number of perforated aluminium plates with two different thicknesses and various perforation ratios. As seen from Eq. (30), the experiment requires mechanical measurements to obtain the spatially averaged squared velocity $\overline{\langle |v_{mn}|^2 \rangle}$ and also acoustical measurements for the radiated sound power W.

The realization of an ideal simply supported boundary condition in practice is not easy. However, several attempts have been made in previous measurements involving this type of boundary condition [26,27]. For this purpose, to support aluminium plates having dimensions of 0.4×0.3 m with 1.5 and 3 mm thicknesses, a 460×362 mm frame with 44 mm height was constructed (see Fig. 9). The experiments were also conducted for free–free boundary conditions. For this, the plates were hung using soft ropes from a stiff frame. As the plates were very lightly damped, thin self-adhesive damping patches, made of a rubber material, were attached to parts of one side of the plates to increase their damping.

The mechanical measurements were obtained in terms of mobility with the plate excited by a shaker. The velocity was measured using a scanning laser vibrometer at 81 locations over the plate surface, while the excitation force was measured by a force transducer. From the mobility measurements, the damping loss factors for all the plates were found to be around $\eta=0.01$ on average.

4.2. Reciprocity technique

The acoustical measurement was conducted using a reciprocity technique in a reverberant chamber, where the plate was excited by a diffuse broadband sound field. This technique was chosen to avoid noise from the shaker which could otherwise contaminate the measured sound power. The plate acceleration was measured by an accelerometer at the same point as the force was applied in the mobility measurement.

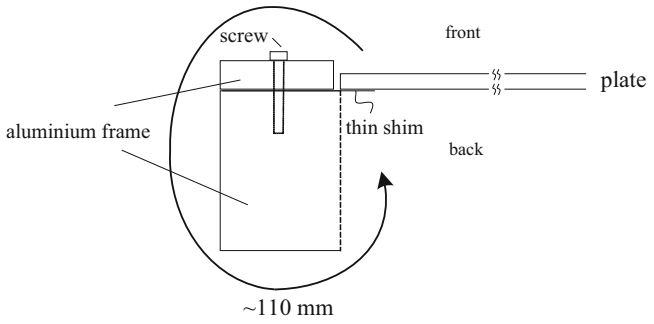

Fig. 9. Mounting arrangement of simply supported plate showing the sound path at the frame edges.

If the direct method experiment is conducted in a reverberant chamber, the radiated power W normalized by the mean-square force $\overline{F^2}$ is given by

$$\frac{W}{\overline{F^2}} = \frac{S\overline{\alpha}}{4\rho c}\left\langle \frac{\overline{p^2}}{\overline{F^2}} \right\rangle \tag{63}$$

where $S\overline{\alpha}$ is the room absorption, ρ is the air density, c is the sound speed and $\langle \overline{p^2} \rangle$ is the spatially averaged mean square pressure in the room due to radiation by the plate. Using the principle of reciprocity, Eq. (63) can then be written as

$$\frac{W}{\overline{F^2}} = \frac{S\overline{\alpha}}{4\rho c}\left\langle \frac{\overline{v_Q^2}}{\overline{Q^2}} \right\rangle \tag{64}$$

where $\overline{v_Q^2}$ is the mean-square plate velocity at the point of excitation (in the direct experiment) due to the sound excitation from a monopole source of mean-square volume velocity $\overline{Q^2}$ from the sound source (in the reciprocal experiment) which is located at the positions used for the microphones in the direct experiment. The spatial average is taken over different source positions. The mean-square volume velocity $\overline{Q^2}$ of a source in a reverberant field at frequency ω is given by [5]

$$\overline{Q^2} = \frac{S\overline{\alpha}\pi}{\rho^2\omega^2}\left\langle \overline{p_Q^2} \right\rangle \tag{65}$$

where $\langle \overline{p_Q^2} \rangle$ is the mean square pressure in the room due to this source. Substituting this into Eq. (64) yields

$$\frac{W}{\overline{F^2}} = \frac{\langle \overline{a_Q^2} \rangle}{\langle \overline{p_Q^2} \rangle}\frac{\rho}{4\pi c} \tag{66}$$

where $a_Q = j\omega v_Q$ is the plate acceleration. In Eq. (66), the mean square acceleration of the plate $\overline{a_Q^2}$ is averaged over sound source positions in the room.

4.3. Measured radiation efficiencies

Fig. 10 presents the radiation index for the 1.5 and 3 mm thick simply supported plates, solid and perforated, along with corresponding predictions in one-third octave bands. Although the measured and predicted results show similar trends, it can be seen that the measured radiation efficiencies exceed the theoretical predictions by about 5–10 dB. However, the measured results show good agreement, particularly at high frequency, with a *baffled* model. For the perforated plate results, this is calculated using a discrete sources approach for a perforated plate in a rigid baffle [5]. This model can only be used for a plate with a small hole density.

When a vibrating plate radiates sound in an unbaffled condition, the radiated sound from one side can 'communicate' with the radiated sound from the other side of the plate. This communication, particularly around the plate edges for a solid plate, creates some cancellation of the sound radiation (see also Section 3.1). The effectiveness of this cancellation depends on the acoustic wavelength; the longer the wavelength the more effective the cancellation. Conversely, in the baffled condition this sort of communication is not possible leading to a higher radiation efficiency.

For the frame used in the experiment, the path length for the sound to propagate from one side of the plate to the other is approximately 110 mm as shown in Fig. 9. In order for the plate to be considered as unbaffled, this has to be less than about half an acoustic wavelength. This is only the case for frequencies less than approximately 1.5 kHz. Above this frequency, the radiated sound from the back of the plate is blocked by the frame and the plate becomes effectively baffled. This may explain the disagreement between the measured results and the unbaffled model, at least above 1 kHz. Moreover, the nature of the radiated sound from the back of the plate is also modified by the frame, so the sound radiation from the back will be more directional than that from the front. This could also reduce the effectiveness of the cancellation process. Hence the plate may be effectively baffled at frequencies lower than 1.5 kHz. Thus it is clear that the frame used for the simply supported boundary conditions does not correspond to an unbaffled situation.

Fig. 11 shows a comparison of the radiation index from measurements for the free–free boundary conditions with that from the analytical calculation for a simply supported plate. It can be seen that a very good agreement is found between the theoretical and the measured results. This raises an interesting finding. It is suggested that, for the case of an unbaffled plate, the radiated sound is relatively insensitive to the edge conditions. To support this it may be observed that calculation of the radiation efficiency of an unbaffled plate with guided boundary conditions shows a difference of less than 2 dB in the corner and edge mode regions compared with that for simply supported edges [5]. Ideally the model developed here for an unbaffled plate should be extended to other plate boundary conditions but this is beyond the scope of the present paper.

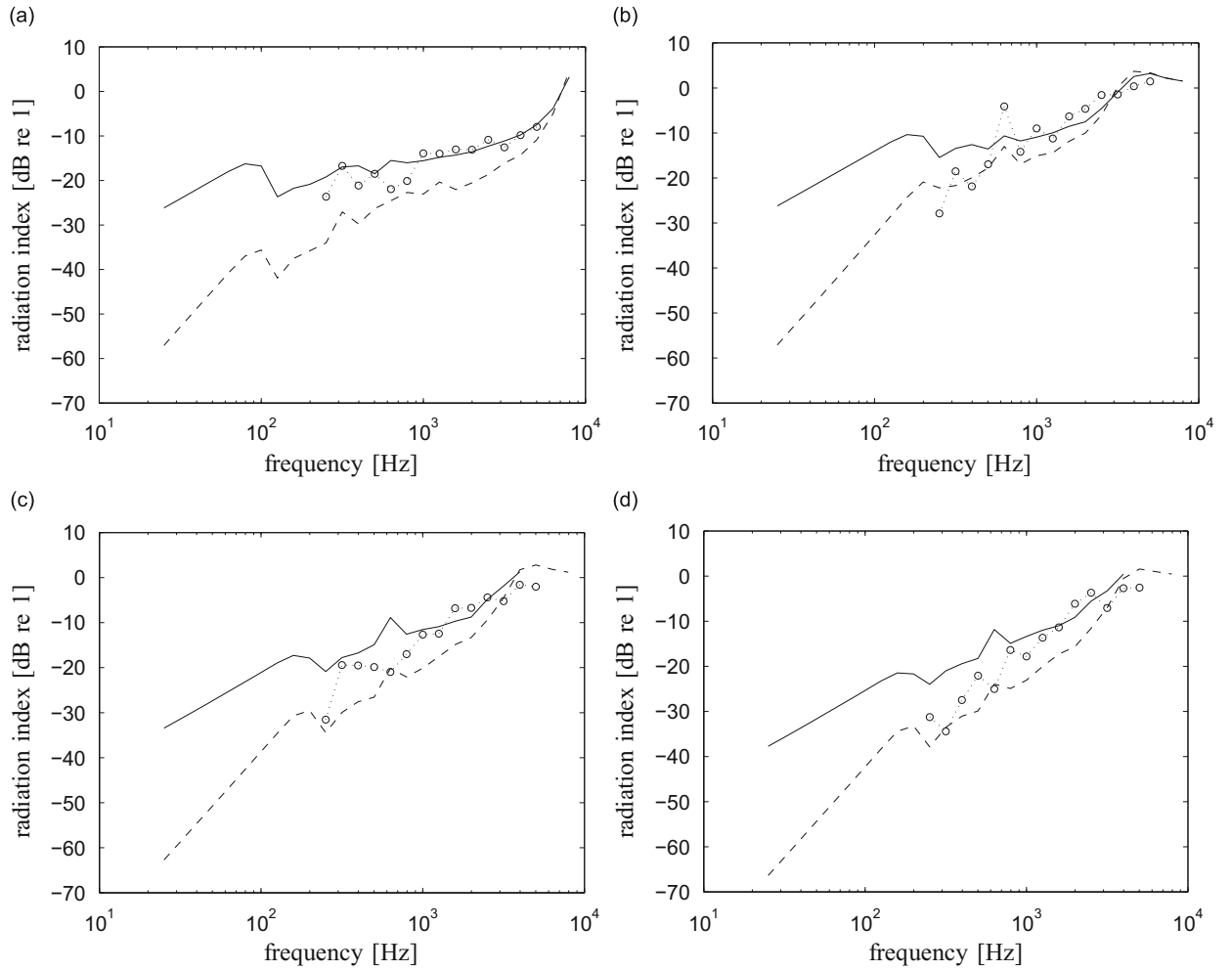

Fig. 10. Measured radiation efficiencies of simply supported unbaffled plates (⋯○⋯): –– unbaffled model, — baffled model; (a) $t=1.5$ mm, unperforated, (b) $t=3$ mm, unperforated, (c) $t=3$ mm, $d_0=15$ mm; $\tau=7$ percent and (d) $t=3$ mm, $d_0=25$ mm; $\tau=20$ percent.

4.4. Measured effect of perforation

Although there are differences between measured results and the model for simply supported plate edges, it is worthwhile to consider the results in the form of the effect of perforation Θ. Fig. 12 compares the effect from analytical calculations with that from measured data of 1.5 and 3 mm thick perforated plates. For the 3 mm plates, the measured data are derived from those presented in Figs. 10(b)–(d) and an additional result for the plate with 10 mm hole diameter and 20 percent perforation ratio. For both thicknesses, the measured data from the simply supported plate experiment can be seen to agree reasonably well with the trend of the model results with roughly 2–5 dB fluctuations above 800 Hz. However, at lower frequencies the fluctuations are greater.

Comparisons are shown for the effect of perforation for the free–free plates in Fig. 13 from the corresponding results in Fig. 11 and also for plates with other perforation configurations. These results show a satisfactory agreement with the predictions, particularly above 400 Hz. The measured results follow the trend of the predictions up to the critical frequency. However, for 1.5 mm thick plates having 5 and 12 percent perforation ratio (Figs. 13(a) and (b)), a disagreement of around 3–5 dB can be seen above 800 Hz. For Fig. 13(b) in particular, this comes from the measured radiation efficiency for the solid plate in Fig. 11(a) where between 800 Hz and 3 kHz the measured result is 1–2 dB lower than the prediction. Conversely, the perforated result (Fig. 11(c)) in the same frequency range is 2–3 dB higher than the prediction, leading to a higher effect of perforation than given by the analytical calculation. This illustrates that it is not easy to obtain a reliable result for Θ because one has to deal with four input errors, i.e. from the sound power and the mobility measurements on both the perforated and the unperforated plates. These errors result in high fluctuations, particularly below 400 Hz where the radiation efficiencies are low, making them subject to noise contamination.

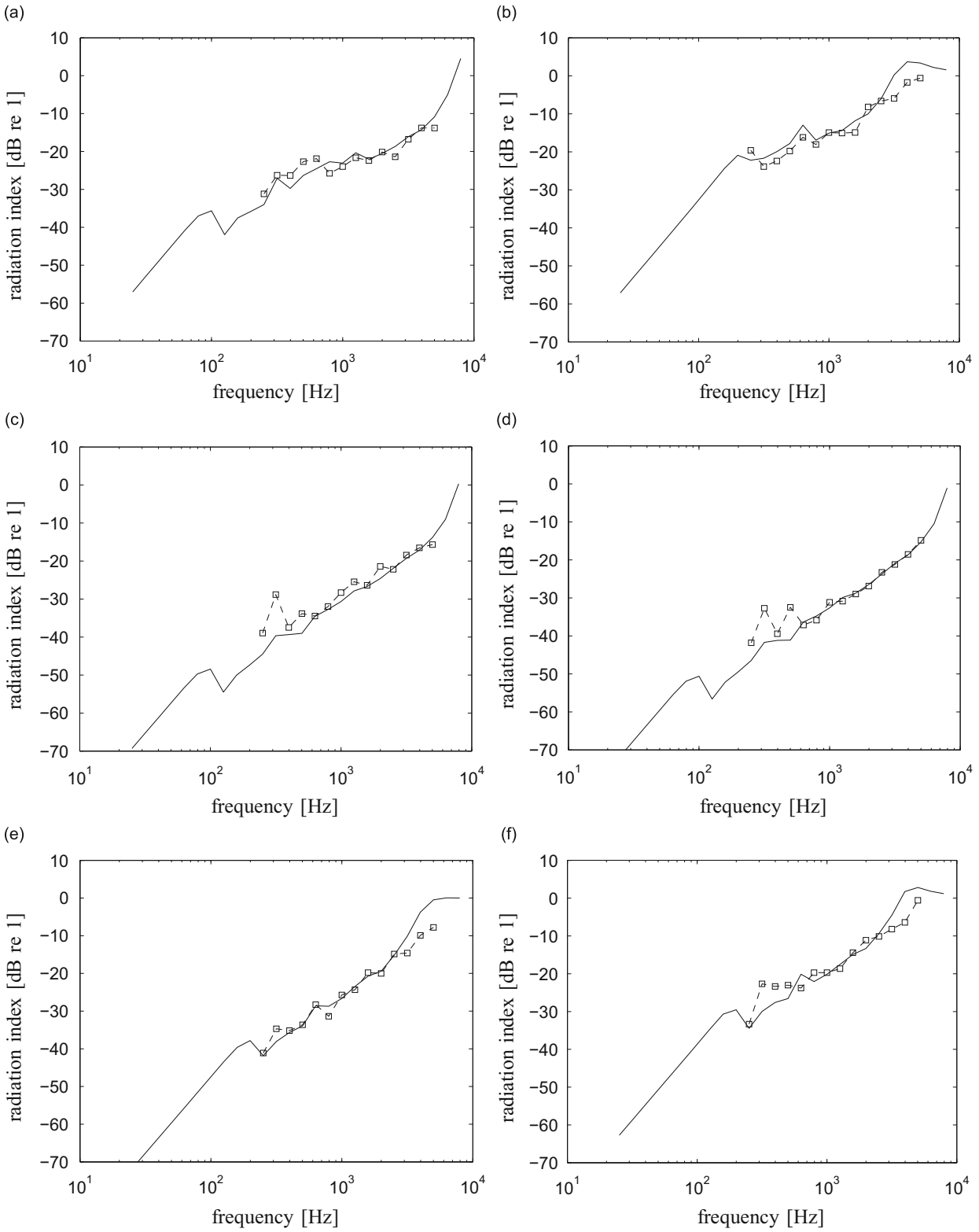

Fig. 11. Measured radiation efficiencies of unbaffled free–free plates (−□−): — unbaffled model (simply supported); (a) t=1.5 mm, unperforated; (b) t=3 mm, unperforated; (c) t=1.5 mm, d_0=8 mm; $\tau = 12$ percent, (d) t=1.5 mm, d_0=10 mm; $\tau = 19$ percent, (e) t=3 mm, d_0=10 mm; $\tau = 20$ percent and (f) t=3 mm, d_0=15 mm; $\tau = 7$ percent.

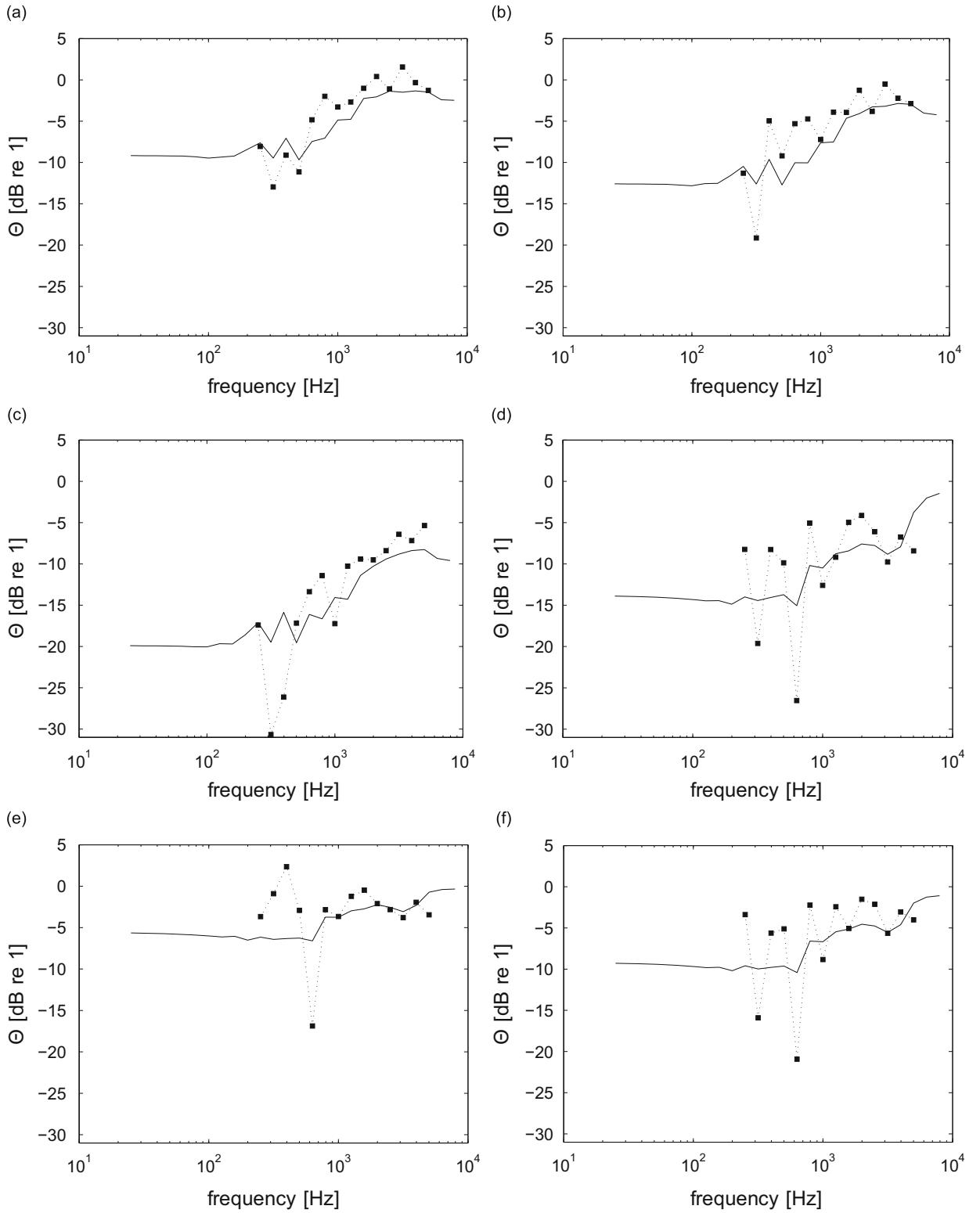

Fig. 12. Measured effect of perforation on unbaffled simply supported perforated plates ($\cdots\square\cdots$): — theoretical; (a) t=1.5 mm, d_0=5 mm, $\tau=5$ percent; (b) t=1.5 mm, d_0=8 mm, $\tau=12$ percent; (c) t=1.5 mm, d_0=15 mm, $\tau=44$ percent, (d) t=3 mm, d_0=10 mm, $\tau=20$ percent, (e) t=3 mm, $d_0=15$ mm, $\tau=7$ percent and (f) t=3 mm, $d_0=25$ mm; $\tau=20$ percent.

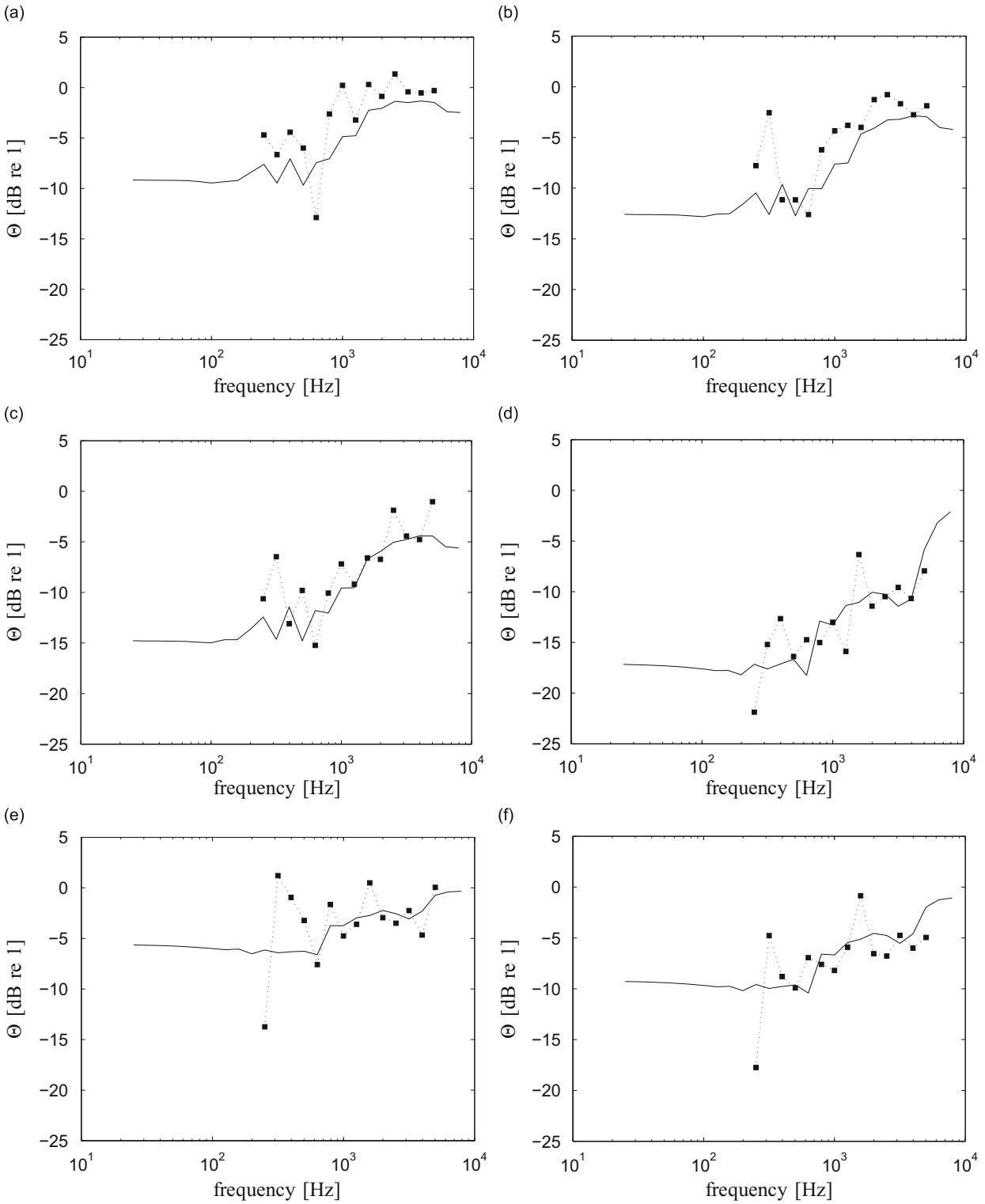

Fig. 13. Measured effect of perforation on unbaffled free-free perforated plates ($\cdots\,\square\,\cdots$): — theoretical (simply supported); (a) t=1.5 mm, $d_0 = 5$ mm, $\tau = 5$ percent; (b) t=1.5 mm, $d_0 = 8$ mm, $\tau = 12$ percent; (c) t=1.5 mm, $d_0 = 10$ mm, $\tau = 19$ percent; (d) t=3 mm, $d_0 = 5$ mm, $\tau = 20$ percent; (e) t=3 mm, $d_0 = 15$ mm; $\tau = 7$ percent and (f) t=3 mm, $d_0 = 25$ mm; $\tau = 20$ percent.

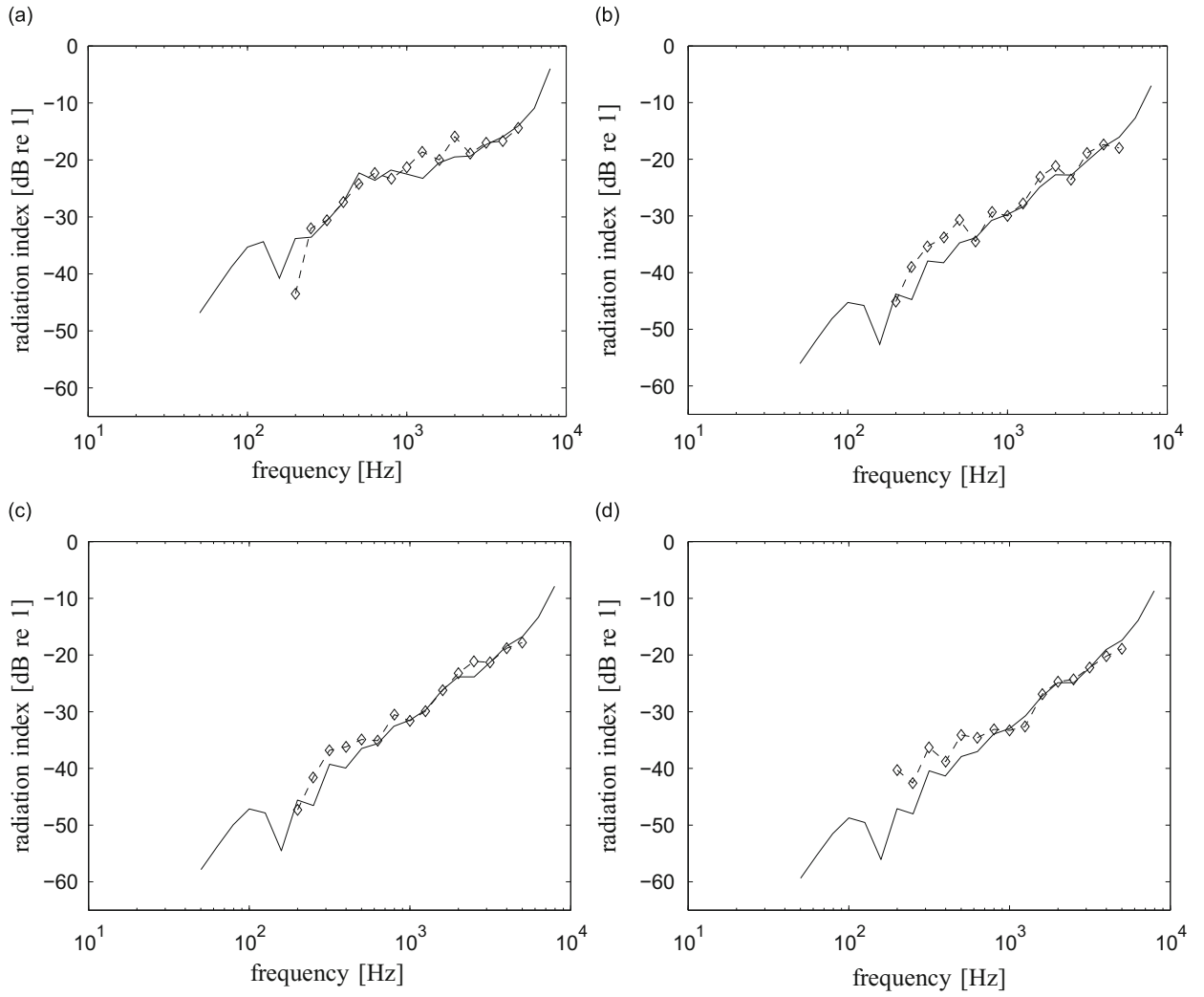

Fig. 14. Comparison of the radiation indices from analytical calculation (—) with those from previous measured data [28] (– ◇ –); (a) unperforated, (b) $d_0 = 5.6$ mm; $\tau = 5.7$ percent, (c) $d_0 = 7.1$ mm; $\tau = 9.4$ percent and (d) $d_0 = 8.8$ mm; $\tau = 14.1$ percent (mild steel; $0.3 \times 0.3 \times 0.0012$ m, $\eta = 0.001$).

4.5. Comparison with existing measured data

To complement the validation of the model, comparison is made with previous measured data. The data were obtained in experiments made by Pierri [28] for 1.22 mm thick perforated steel plates having dimensions of 0.3×0.3 m (also given in [4]). The measurement of the radiation efficiency was conducted using the direct method, where the plate was excited by a broadband force from a shaker and the radiated sound pressure was measured in a reverberant room. The plate sample was supported by the edges with very soft foam rubber so that free–free boundary conditions could be assumed.

Fig. 14 shows a comparison of the measured radiation index with that from the model. The damping loss factor is not known but in the calculation it is assumed to be very low, i.e. $\eta = 0.001$. It can be seen that the measured results agree very well with the model, including the case of the unperforated plate.

5. Approximate formula for effect of perforation

In practice, rather than the absolute level of sound power (or radiation efficiency) of a perforated structure, the level of noise reduction due to perforation is often of interest. Therefore in this section a simple empirical formula is derived that can be used as quantitative guidance for an engineering application to predict the noise reduction.

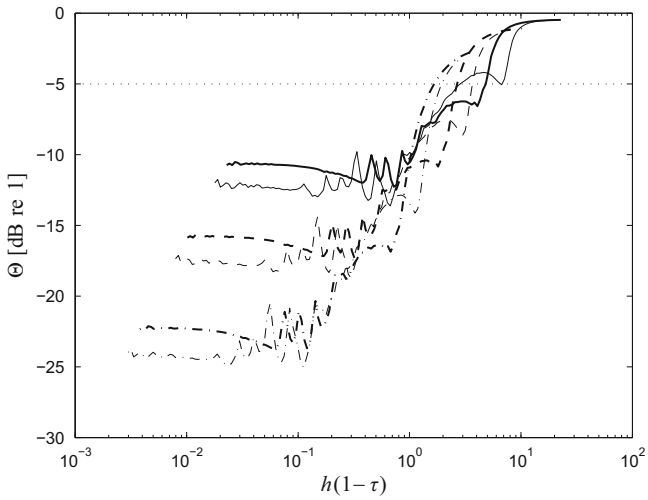

Fig. 15. Effect of perforation on sound power radiation of a simply supported perforated unbaffled plate plotted against h ($0.65 \times 0.5 \times 0.003$ m (thin lines), $0.65 \times 0.5 \times 0.006$ m (thick lines)), aluminium plate with $\eta = 0.1$, $d_0 = 10$ mm: $\tau =$ — 10 percent, – – 20 percent, – · – 40 percent, · · · 60 percent).

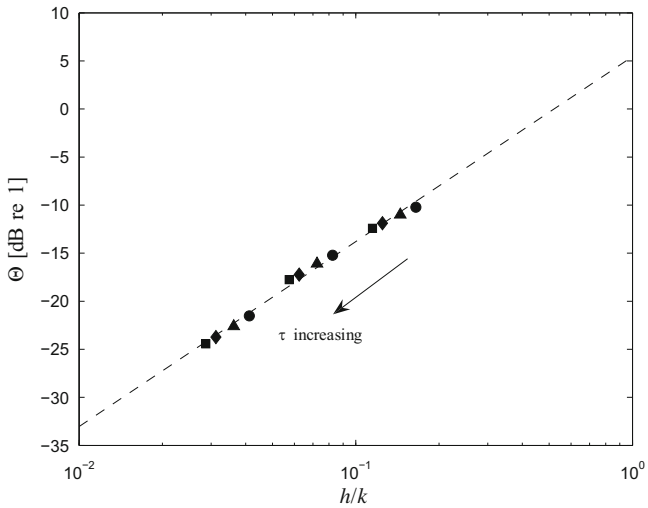

Fig. 16. Effect of perforation on sound power radiation of a simply supported perforated unbaffled plate at low frequency asymptote for different thickness (□: $0.65 \times 0.5 \times 0.003$ m, ◇: $0.65 \times 0.5 \times 0.004$ m, △: $0.65 \times 0.5 \times 0.006$ m, ◦: $0.65 \times 0.5 \times 0.008$ m aluminium plate with $\eta = 0.1$, $d_0 = 10$ mm; $\tau = 10$,20 and 40 percent).

5.1. Edge mode region

Fig. 15 plots the predicted effect of perforation for the various cases considered against the non-dimensional specific acoustic reactance h for different plate thicknesses. It can be seen that the curves collapse together with the same slope of 15 dB/decade in the edge mode region. Below the edge mode region, the results are independent of h but vary with plate dimensions and perforation ratio.

In the edge mode region, up to half the critical frequency, the effect of perforation Θ can be written as

$$\Theta = 15 \log_{10}[h(1-\tau)] - 10, \quad f_e < f < f_c/2 \tag{67}$$

where f_e is the starting frequency of the edge mode region and f_c is the critical frequency as given in Eqs. (60) and (61), respectively. Note that this is valid only for reductions of more than 5 dB. For smaller reductions, the curve becomes less steep as it approaches 0 dB.

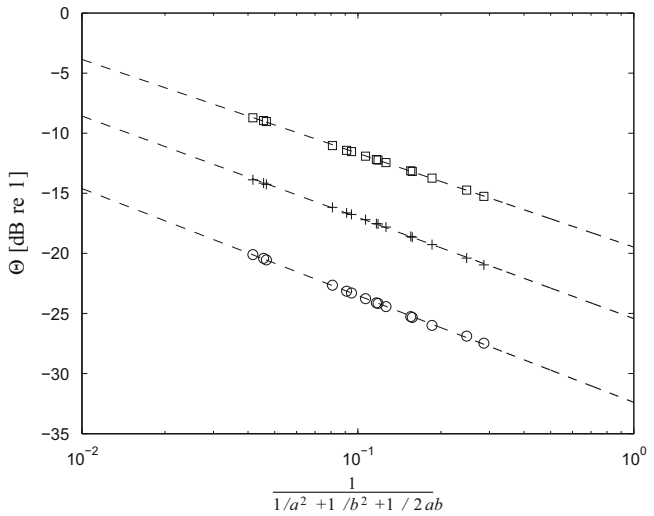

Fig. 17. Effect of perforation on sound power radiation of a simply supported perforated unbaffled plate at low frequency asymptote for various plate dimensions (t=3 mm, aluminium plate with $\eta = 0.1$; □ = 10 percent, + = 20 percent, ∘ = 40 percent).

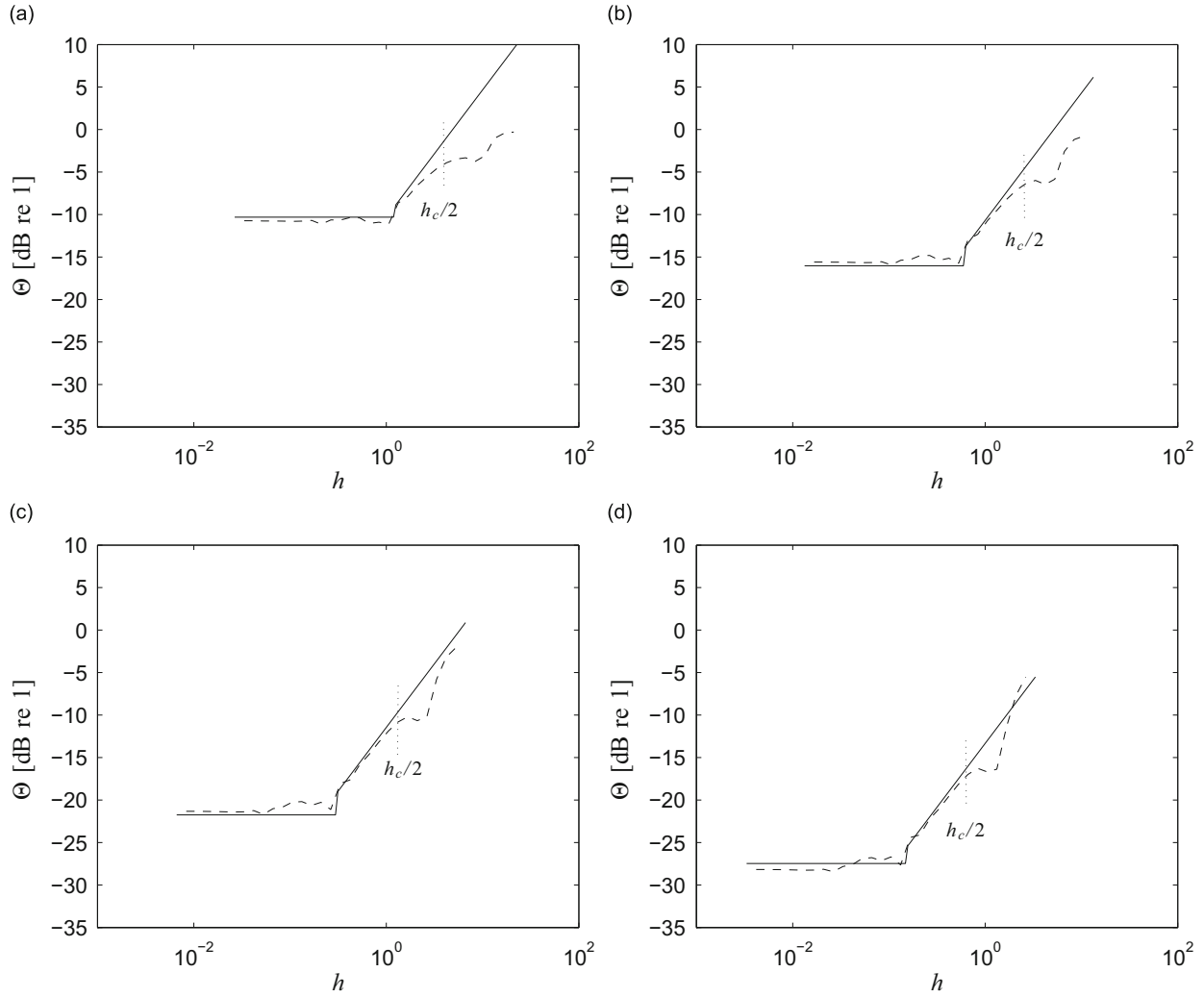

Fig. 18. Effect of perforation on sound power radiation of a simply supported perforated unbaffled plate: 0.65 × 0.5 × 0.003 m; (a) $\tau = 5$ percent, (b) $\tau = 10$ percent, (c) $\tau = 20$ percent, (d) $\tau = 40$ percent; −− analytical, — prediction (aluminium plate with $\eta = 0.1$, $d_0 = 5$ mm).

5.2. Fundamental and corner mode regions

From Figs. 8(c) and (d) and Fig. 15, as the effect shows almost constant values at low frequency, at least up to end of the corner mode region, an approximate formula can be developed to predict the effect of perforation in this frequency region.

Fig. 16 plots the effect of perforation at low frequency for plates with the same dimensions but different thickness and perforation ratio to show the increment in the Θ as the plate thickness increases. This is plotted against h/k, which is independent of frequency. The constant values over the corner mode region are, in this case, taken from the average value between 10 and 30 Hz in each case. It is seen that the perforation of thinner plates has a greater effect of reducing the sound radiation. This is reflected in the dependence of h on t (see Eq. (7)). The result also shows that the trend has a dependency of about 19 dB/decade. Therefore a simple curve fit can be obtained as a function of the non-dimensional acoustic reactance h

$$\Theta \approx 19 \log_{10}\left(\frac{h}{k}\right) + 5, \quad f < f_e \tag{68}$$

The effect of perforation at low frequency for different dimensions with the same plate thickness is shown in Fig. 17 for perforation ratios of 20 and 40 percent. For the 20 percent perforation ratio, the dependence on the plate dimensions a and b can be written as

$$\Theta \approx -8.5 \log_{10}\left(\frac{1}{1/a^2 + 1/b^2 + 1/2ab}\right) - 25.5, \quad f < f_e \tag{69}$$

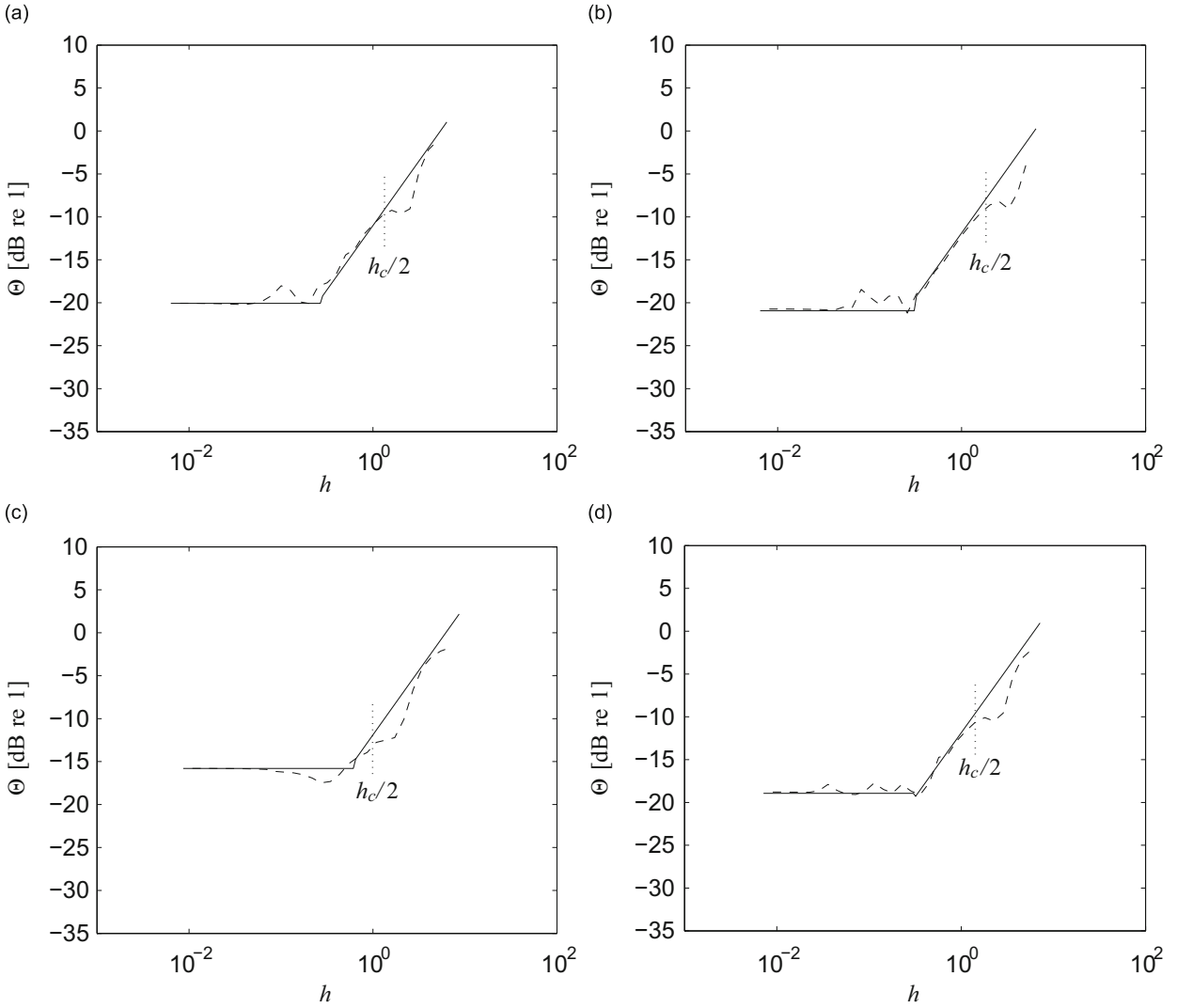

Fig. 19. Effect of perforation on sound power radiation of a simply supported perforated unbaffled plate: $\tau = 25$ percent; (a) $0.8 \times 0.4 \times 0.003$ m, (b) $0.65 \times 0.4 \times 0.002$ m, (c) $0.39 \times 0.3 \times 0.005$ m and (d) $0.9 \times 0.3 \times 0.003$ m; –– analytical, — prediction (aluminium plate with $\eta = 0.1$, $d_0 = 8$ mm).

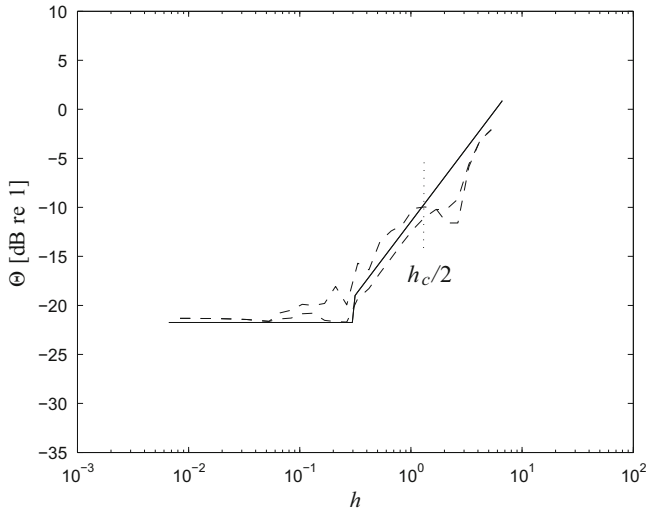

Fig. 20. Effect of perforation on sound power radiation of a simply supported perforated unbaffled plate: $d_0 = 5$ mm, $\tau = 20$ percent; $-\cdot-\eta = 0.001$, $--\eta = 0.2$, — prediction (aluminium plate).

where a and b are given in metres (m). The results for 10 and 40 percent perforations have similar gradients to that for 20 percent, but different constant terms.

These two equations (Eqs. (68) and (69)) can be combined to give a general equation for the effect of perforation at low frequency:

$$\Theta = -8.5\log_{10}\left(\frac{1}{1/a^2+1/b^2+1/2ab}\right)+19\log_{10}\left(\frac{h}{k}\right)-2, \quad f<f_e \tag{70}$$

Figs. 18 and 19 show a comparison of the effect of perforation to test the validity of Eqs. (67) and (70) for different perforation ratios, plate dimensions and thickness. Results are shown in Fig. 18 for the same plate size with 5 mm hole diameter and different perforation ratios. Fig. 19 shows the effect for different plate size with 8 mm hole diameter and 25 percent perforation ratio. For clarity, these are plotted in one-third octave bands. The results show good agreement over the frequency range up to half the critical frequency. However in the corner mode region, the approximate model does not give such a good estimation. This is due to large fluctuations in this region both from the radiation efficiency of the perforated plate and that of the solid plate, which then also lead to large fluctuations in the 'effect of perforation' curve. Nevertheless the differences in this region are only 2–3 dB at most and the model can be used to good effect. Fig. 18(a) also shows an over-prediction just before $h_c/2$ as the sound reduction is less than 5 dB in that frequency range (see Section 5.1). Fig. 20 presents a comparison for two extreme values of damping loss factor ($\eta = 0.001$ and 0.2) again showing good agreement with the model.

6. Conclusions

The sound radiation from a perforated plate has first been calculated using an approach from Fahy and Thompson [2] in which the plate is assumed to be set in a rigid perforated baffle. The model is based on the assumption that the baffle has similar perforation to the plate in order to have a continuous impedance across the plate and the baffle for convenience of calculation. It has been shown that, according to this model, the radiation efficiency of the baffled plate is considerably reduced at low frequency due to the perforation. However, this is more due to the effect of perforation of the baffle rather than due to perforation of the plate itself.

A model for an unbaffled perforated plate has therefore been developed by extending Laulagnet's model for the radiation efficiency of an unbaffled solid plate [10]. The perforation leads to a reduction in the radiation efficiency which is constant at low frequencies (up to the corner mode region) and decreases as the frequency approaches the critical frequency.

Comparing the results from the two models, it has been found that the simpler model can be used to predict the radiation for the unbaffled case fairly reliably for moderate perforation ratios (around 20 percent). This approach has the advantage of a much reduced computational effort.

It is found from both models that the sound radiation reduces as the perforation ratio is increased or the hole size is reduced. The effect also depends on the plate thickness and dimensions. For only 10 percent perforation ratio and 10 mm diameter holes, the sound radiation can be reduced by 10–15 dB at low frequencies, which illustrates the effectiveness of perforation as a noise control measure. An approximate formula to predict the effect of perforation has also been proposed which can be used for frequencies up to half the critical frequency.

Comparison of the model with experimental results for a series of freely suspended perforated plates gives a good agreement, even though the model has been based on simply supported boundary conditions.

References

[1] Anonymous, *Noise Control: Principles and Practice*, Brüel & Kjær, Naerum, Denmark, 1986.
[2] F.J. Fahy, D.J. Thompson, The effect of perforation on the radiation efficiency of vibrating plates, *Proceedings of the Institute of Acoustics* 26 (2004).
[3] D.Y. Maa, Theory and design of microperforated panel sound absorbing constructions, *Scientia Sinica* 18 (1975) 55–71 (in Chinese).
[4] F.J. Fahy, P. Gardonio, *Sound and Structural Vibration: Radiation, Transmission and Response*, second ed., Academic Press, London, 2006.
[5] A. Putra, Sound Radiation from Perforated Plates, Ph.D. Thesis, ISVR, University of Southampton, 2008.
[6] E.G. Williams, Numerical evaluation of the radiation from unbaffled, finite plates using the FFT, *Journal of the Acoustical Society of America* 74 (1983) 343–347.
[7] N. Atalla, J. Nicolas, C. Gauthier, Acoustic radiation of an unbaffled vibrating plate with general elastic boundary conditions, *Journal of the Acoustical Society of America* 99 (1996) 1484–1494.
[8] C.H. Oppenheimer, S. Dubrowsky, A radiation efficiency for unbaffled plates with experimental validation, *Journal of Sound and Vibration* 199 (1997) 473–489.
[9] H. Nelisse, O. Beslin, J. Nicolas, A generalized approach for the acoustic radiation from a baffled or unbaffled plate with arbitrary boundary conditions immersed in a light or heavy fluid, *Journal of Sound and Vibration* 211 (1998) 207–225.
[10] B. Laulagnet, Sound radiation by a simply supported unbaffled plate, *Journal of the Acoustical Society of America* 103 (1998) 2451–2462.
[11] M.H.A. Janssens, W.J. van Vliet, Noise from steel bridges: research into the effect of perforations of bridge components, Technical Report, TNO Report TPD-HAG-RPT-960057, 1996 (in Dutch).
[12] D. Takahashi, M. Tanaka, Flexural vibration of perforated plates and porous elastic materials under acoustic loading, *Journal of the Acoustical Society of America* 112 (2002) 1456–1464.
[13] M. Toyoda, D. Takahashi, Reduction of acoustic radiation by impedance control with a perforated absorber system, *Journal of Sound and Vibration* 286 (2005) 601–614.
[14] M. Toyoda, M. Tanaka, D. Takahashi, Reduction of acoustic radiation by perforated board and honeycomb layer systems, *Applied Acoustics* 68 (2007) 71–85.
[15] D.Y. Maa, Microperforated panel wideband absorber, *Noise Control Engineering Journal* (1987) 77–84.
[16] T. Dupont, G. Pavic, B. Laulagnet, Acoustic properties of lightweight micro-perforated plate systems, *Acta Acustica United with Acustica* 89 (2003) 201–212.
[17] Y.Y. Lee, E.W.M. Lee, C.F. Ng, Sound absorption of a finite flexible micro-perforated panel backed by an air cavity, *Journal of Sound and Vibration* 287 (2005) 227–243.
[18] K. Sakagami, M. Morimoto, W. Koike, A numerical study of double-leaf microperforated panel absorbers, *Applied Acoustics* 67 (2006) 609–619.
[19] A.D. Pierce, *Acoustics*, Acoustical Society of America, Melville, NY, 1989.
[21] L. Cremer, M. Heckl, B.A.T. Petersson, *Structure-borne Sound*, third ed., Springer, Berlin, 2005.
[22] G. Xie, D.J. Thompson, C.J.C. Jones, The radiation efficiency of baffled plates and strips, *Journal of Sound and Vibration* 280 (2005) 181–209.
[23] M.C.M. Wright, *Mathematics of Acoustics*, Imperial College Press, London, 2005.
[24] W.L. Li, H.J. Gibeling, Determination of the mutual radiation resistances of a rectangular plate and their impact on the radiated sound power, *Journal of Sound and Vibration* 229 (2000) 1213–1233.
[25] L.L. Beranek, *Noise and Vibration Control*, McGraw-Hill, New York, 1971.
[26] J.B. Ochs, J.C. Snowdown, Transmissibility across simply supported thin plates. I. Rectangular and square plates with and without damping layers, *Journal of the Acoustical Society of America* 58 (1975) 832–840.
[27] O. Lacour, M.A. Galland, D. Thenail, Preliminary experiments on noise reduction in cavities using active impedance changes, *Journal of Sound and Vibration* 230 (2000) 69–99.
[28] R.A. Pierri, Study of a Dynamic Absorber for Reducing the Vibration and Noise Radiation of Plate-like Structures, M.Sc. Dissertation, ISVR, University of Southampton, 1977.